



Schweizerische Eidgenossenschaft
Confédération suisse
Confederazione Svizzera
Confederaziun svizra

Federal Department of the Environment, Transport,
Energy and Communications DETEC

Swiss Federal Office of Energy SFOE
Energy Research and Cleantech Division

Final report dated 14.12.2020

“Intelligent SCR” (INTSCR)



Date: 14.12.2020

Location: Bern

Publisher:

Swiss Federal Office of Energy SFOE
Energy Research and Cleantech
CH-3003 Bern
www.bfe.admin.ch

Subsidy recipients:

Paul Scherrer Institut (PSI)
Energy and Environment
OVGA/119, Forschungsstrasse 111, CH-5232 Villigen PSI
www.psi.ch

Hug Engineering AG
Im Geren 14, CH-8352 Elsau
www.hug-eng.ch

Vir2sense GmbH
Sihlbruggstrasse 109, CH-6340 Baar
www.vir2sense.com

Authors:

B. von Rotz, Paul Scherrer Insitut, beat.von-rotz@psi.ch
A. Marberger, Hug Engineering, adrian.marberger@hug-engineering.com
D. Gschwend, Hug Engineering, dominik.gschwend@hug-engineering.com
C. Barro, Vir2sense, barro@vir2sense.com
P. Kyrtatos, Vir2sense, kyrtatos@vir2sense.com

SFOE project coordinators:

Luca Castiglioni, luca.castiglioni@bfe.admin.ch

SFOE contract number: SI/501738-01

The authors bear the entire responsibility for the content of this report and for the conclusions drawn therefrom



Zusammenfassung

Moderne Verbrennungsmotoren mit elektronischer Steuerung ermöglichen einen direkten Zugriff auf den Motorbetrieb. Dies eröffnet die Möglichkeit zu einer neuartigen aktiven SCR-basierten Motorsteuerung, wobei die NO_x-Emissionen vom Motor in einer Konzentration emittiert werden, welche basierend auf der tatsächlichen Verfügbarkeit des Ammoniaks im SCR-Katalysators auch umgewandelt werden können. Dieses Konzept hat den Vorteil, dass die Abgasreinigungsanlage stets optimal ausgelastet ist. Dies erlaubt wiederum einen effizienteren Motorbetrieb in allen Betriebspunkten. Diesbezüglich wurde der Grossmotorenprüfstand am PSI mit umfangreicher Messtechnik im Abgastrakt und Abgasnachbehandlungssystem ausgestattet und zusätzliche Steuerungssysteme implementiert. Der SCR Status wird mit Hilfe eines NO_x-Umsatz und Ammoniakspeichermodells, welches mit Labormessungen kalibriert wurde, abgerufen. Für die Realisierung solch einer Steuerung müssen die aktuell mögliche Umwandlungsraten sowie das Ursachen-Wirkung-Prinzip zwischen Änderungen der Einspritzparameter (Einspritzdruck, Einspritzbeginn) oder Luftpfadparameter (Wastegate) und den Änderungen in den NO_x-Emissionen bekannt sein. Ein «physically-assisted virtual sensor» fungiert dabei als Schnittstelle zwischen Katalysator und Motor.

Das Projekt konnte den Proof-of-concept dieser Technologie erbringen. Brennstoffersparnisse im Bereich von ca. 1% bei zeitgleicher Reduktion von Reingas NO_x sowie Minimierung des Ammoniakschlupfes. Die Technologie zeigt Potential im Bereich der mittelschnellen und langsamlaufenden Motoren mit Abgasnachbehandlungssystemen, welche im Bereich der marinen Antriebsysteme oder als stationäre Energieerzeuger eingesetzt werden. Letztere z.B. für die schnelle Bereitstellung von Energie für die Netzstabilität.

Résumé

Les moteurs modernes à commande électronique permettent un accès direct au fonctionnement du moteur. Cela ouvre la possibilité d'un nouveau type de contrôle du moteur basé sur la SCR, dans lequel les émissions de NO_x sont émises par le moteur dans une concentration qui peut également être convertie en fonction de la disponibilité réelle de l'ammoniac dans le convertisseur catalytique SCR. Ce concept présente l'avantage que le système de purification des gaz d'échappement est toujours utilisé de manière optimale. Cela permet un fonctionnement plus efficace du moteur à tous les égards. À cet égard, le grand banc d'essai de moteurs du PSI a été équipé d'une technologie de mesure étendue dans le système d'échappement et de post-traitement des gaz d'échappement et d'autres systèmes de contrôle ont été mis en place. Le statut SCR est obtenu à l'aide d'un modèle de conversion des NO_x et de stockage de l'ammoniac, qui a été calibré avec des gènes de mesure de laboratoire. Pour la réalisation d'un tel système de contrôle, il faut connaître le taux de conversion réel possible ainsi que le principe de cause à effet entre les modifications des paramètres d'injection (pression d'injection, début d'injection) ou des paramètres de la voie aérienne (wastegate) et les modifications des émissions de NO_x. Un "capteur virtuel assisté physiquement" sert d'interface entre le catalyseur et le moteur.

Le projet a pu fournir une preuve de concept de cette technologie. Économies de carburant de l'ordre d'environ 1% avec réduction simultanée des NO_x des gaz propres et minimisation du glissement de l'ammoniac. Cette technologie présente un potentiel dans le domaine des moteurs à vitesse moyenne et lente avec systèmes de post-traitement des gaz d'échappement, qui sont utilisés dans les systèmes de propulsion marine ou comme générateurs d'énergie stationnaires. Ce dernier, par exemple, pour la fourniture rapide d'énergie pour la stabilité du réseau.



Summary

Modern combustion engines with electronic control allow direct access to the engine operation. This enables the possibility of a new type of SCR-based engine control, whereby NO_x emissions are emitted by the engine in a concentration, which can also be converted based on the actual availability of ammonia in the SCR catalytic converter. This concept has the advantage that the exhaust gas aftertreatment system is always optimally utilized. This allows more efficient engine operation throughout all conditions. Therefore, the large engine test bench at PSI was equipped with extensive measurement technology in the exhaust tract and exhaust aftertreatment system as well as advanced control systems were implemented. The SCR status is retrieved with the help of a NO_x conversion and ammonia storage model, which was calibrated with laboratory measurements. For the realization of such a control system the actual possible conversion rate as well as the cause-effect principle between changes in injection parameters (injection pressure, injection start) or air path parameters (wastegate) and the changes in NO_x emissions must be known. A "physically-assisted" virtual sensor acts as an interface between the catalyst and the engine.

The project was able to provide proof-of-concept of this technology. Fuel savings in the range of approx. 1% with simultaneous reduction of tail pipe NO_x and minimization of ammonia slip. The technology shows potential in the field of medium and low-speed engines with exhaust aftertreatment systems, which are used in marine propulsion systems or as stationary power generator application. The latter e.g. for the quick supply of energy for grid stability.

Main findings

- Development and implementation of an advanced "intelligent" engine/SCR control system for stationary and transient engine operation
- Elaboration of a SCR storage/conversion model as well as further development of PVS based control systems (incl. virtual engine setup)
- Pilot application of the "intelligent" SCR system, demonstrating lowered fuel consumption and thus CO₂ emissions (0.8% reduction vs reference cycle), and simultaneously reduced tail pipe NO_x emissions (>50% reduction) and ammonia slip (60% reduction)
- Contribution to minimize the GHG emissions for medium and low-speed engines with SCR aftertreatment systems



Contents

1	Introduction	8
1.1	Background information and current situation.....	8
1.2	Purpose of the project.....	8
1.3	Objectives.....	8
2	Description of facility	9
2.1	Description of the LERF.....	9
2.2	Description of the exhaust gas after treatment system.....	12
3	Procedures and methodology	15
3.1	Description of the test cycle.....	15
3.2	Description of the SCR control strategies.....	17
3.3	SCR Model.....	19
	Modelling.....	19
3.3.1	Reaction Kinetics Experiments – Setup.....	19
3.3.2	Reaction Kinetics Experiments - Measurement.....	20
3.3.3	Reaction Kinetics Experiments - Measurement.....	20
3.3.4	Reaction Kinetics Experiments – general procedure.....	21
3.3.5	Parameter Determination.....	22
3.4	Optimization procedure.....	23
3.4.1	Virtual engine testbench.....	23
3.4.2	Engine operation optimization:.....	23
4	Results and discussion	29
4.1.1		
4.1.2	4.1 SCR model.....	29
	Model parameters.....	29
4.3.1	SCR modelling.....	29
4.3.2	4.2 Virtual Testbench.....	30
4.3.3		
4.3.4	4.3 Results dosing table & feed forward control.....	33
	Map based control (<i>DT</i>).....	33
4.4.1	Feed forward control (<i>FF-0.9</i>).....	35
4.4.2	Feed forward control (<i>FF-0.95</i>).....	37
	Feed forward control (<i>FF-PVS</i>).....	39
4.4	4.4 Results after optimization.....	41
	Offline optimization.....	41
	Hybrid off/online optimization <i>Hyb Opt</i>	43
4.5	4.5 Cycle comparison:.....	49
5	Conclusions	58
6	Outlook and next steps	59



7	National and international cooperation.....	61
8	Publications	61
9	References	61



Abbreviations

ECU	Electronic/Engine Control Unit
LERF	Large Engine Research Facility
PVS	Physically-assisted Virtual Sensor
SCR	Selective Catalytic Reduction
SOI	Start of Injection
VIC	Variable Intake Cam
WG	Wastegate



1 Introduction

1.1 Background information and current situation

The optimum operation of diesel engines always displays a trade-off behavior between fuel consumption and emissions. This trade-off is 3-dimensional and includes the quantities of soot / PM emissions, NO_x emissions and fuel consumption / CO₂ emissions. Normally, the emissions of soot and fuel consumption increase when NO_x emissions decrease. Consequently, an increase in the efficiency of the NO_x emission reduction system (selective catalytic reduction, SCR) is often accompanied by a reduction in fuel consumption, and thus CO₂ emissions. So far, in large diesel engine applications the engine as well as the SCR system are operated as separate units (especially in off-road, marine and stationary power generation applications). The development of an intelligent SCR system, whereby the engine and the SCR control systems communicate, enables the possibility for an overall optimization (engine and exhaust aftertreatment in combination).

1.2 Purpose of the project

The purpose of the project is to develop the technology and sub-systems (in particular virtual sensors and SCR-storage/conversion models) which will allow the integration of the engine and SCR control systems, in order to enable a low-emission and efficient operation of medium and low speed diesel engines. This system will allow the combined optimization of the engine and exhaust aftertreatment system, enabling compliance to existing and upcoming emission regulations while minimizing fuel consumption and CO₂ emissions.

1.3 Objectives

The application of the intelligent SCR system will be developed and tested in the Large Engine Research Facility (LERF) of the PSI in Villigen, which houses a state of the art, Common Rail, medium speed diesel engine. The project is divided into three phases: In a first phase, the testbench is adapted to the requirements, including the installation of a new SCR catalyst setup, while the Physically-assisted Virtual Sensor (PVS) needs to be adapted for the engine used. The PVS is a model-based emission monitoring system will provide a continuous signal of engine-out NO_x emissions independent of the engine operating conditions, without the need for direct measurement of the emissions. The goals of the first phase are to acquire reference measurements, the definition of a transient operating cycle and a run of this cycle with a map-based SCR control as a benchmark. In the second phase, a feedforward controller needs to be integrated into the SCR control system to dose urea according to the actual emissions instead of the map-based system used in phase 1. The signal of the real-time emissions in phase 2 is provided by the PVS. The cycle with this setup is compared with the benchmark as well as with a run in which the emissions for the SCR feedforward control are provided by a physical sensor. In the second phase, the PVS only outputs NO_x freight even though the entire high-pressure cycle calculation is performed and available. To make use of this calculation, in the third phase, the PVS is used to provide the required engine settings (start of injection, waste gate position etc.) to allow optimum SCR performance by controlling the NO_x freight in real time. The set point values of NO_x freight for the optimum SCR performance are determined using an SCR storage/conversion model



2 Description of facility

2.1 Description of the LERF

The test engine with the Hug Engineering SCR system (combiKat[®]) is located at the LERF of PSI. The facility was designed and built for research into low emission technologies as well as new turbocharging and combustion concepts on large marine and stationary diesel engines. Furthermore, the LERF is enabling investigations regarding sensor technologies and monitoring systems for diesel engine combustion systems. Additionally, the installation can facilitate studies related to energy system integration approaches by acting as an appropriate reference data source for the corresponding modelling/simulation development.

The test engine installed is an in-line 6 cylinder Wartsila 6L20CR, 4-stroke, medium speed Diesel engine with a common rail fuel injection system from L'Orange GmbH (now Woodward L'Orange). Table 1 shows the main specifications of the test engine:

Table 1: W6L20CR Engine Specification

Bore	<i>mm</i>	200
Stroke	<i>mm</i>	280
Number of Cylinders		6
Displacement Volume	<i>l</i>	8.8 (52.8)
Compression Ratio		16
Nominal Speed	<i>rpm</i>	1000
Rated Power	<i>kW</i>	1080 (1278 kVA)

The existing control and measurement equipment allow steady-state and transient exhaust analysis, as well as fast in-cylinder and manifold pressure measurement. The engine has been modified to allow variable inlet closure by adjusting the valve timing (Miller cycle). Furthermore, the original (single) turbo charger system has been changed to a prototype two-stage turbocharger system (from ABB Turbo Systems Ltd), to be able to achieve higher boost pressures in order to compensate the power output reduction caused by the earlier inlet valve closure when operating the engine on Miller cycle conditions. Moreover, an exhaust gas recirculation system is installed, where exhaust gas can be redirected in a so-called semi-short-route configuration where the gases are introduced into the intake air path after the low-pressure and before the high-pressure compressor of the turbocharging system. Lately, the installation has been upgraded with a waste gate valve, which is enabling the bypass of the turbocharging system by directing the exhaust gases before the high-pressure turbine directly into the exhaust pipe. Both measures can directly influence the engine out NO_x emissions and are therefore, highly interesting for the project scope as a control parameter.

An overview of test engine and plant facilities can be seen in Figure 1. More information about the engine setup and past experiments can be found in [1-8].



Figure 1: View of the LERF test engine and SCR-system

The control and data acquisition system at the engine test bed is an essential part in order to fulfil the aim of the project to interconnect the engine and the SCR system.

After the assessing and analysing the needs of each partner with the corresponding systems (PVS, SCR, engine), the control as well as acquisition system have been upgraded, accordingly. A complete new additional subsystem has been installed in the LERF facility and has been integrated into the existing engine and facility control system. It enables the recording of all relevant conditions measured or important control parameters. The SPS-based system is connected via different communication protocols (Modbus, CAN) to the various control systems. The additional acquisition system is finally operated in an OPC UA environment and is storing the all the data via a LabView script on a server with a sampling frequency of 1 Hz. Any additional client such as the PVS system can be integrated via this Open Communication Protocol to read and, if necessary, write parameters on to the data server.

The newly data acquisition system is facilitating the operation of the engine and SCR system in combination and during the engine/SCR testing all needed data can be visualized real-time as well as recorded for the further analysis and modelling purposes.

Figure 2 shows a schematic overview of the new control and data acquisition systems at the LERF.

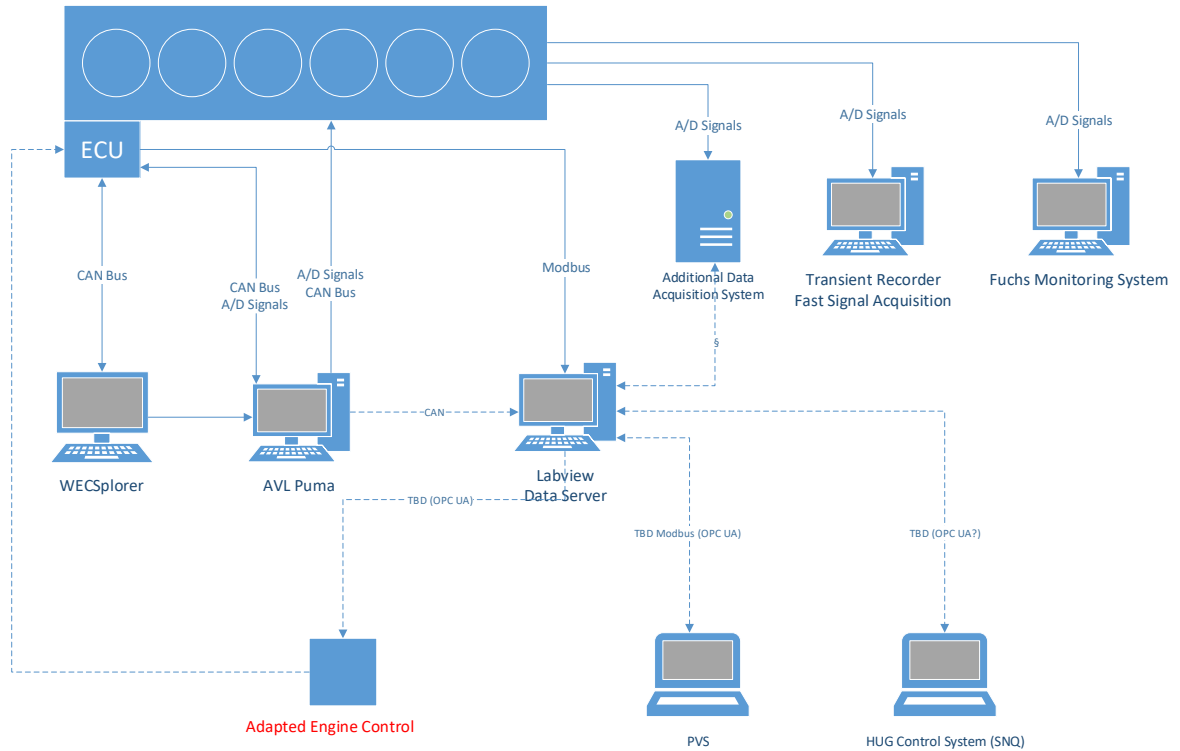


Figure 2: Schematic of the control and data acquisition system at the test bed with an additional external control system such as the PVS from Vir2sense as well as a new adapted engine control system

A very versatile and well instrumented state-of-the-art test facility has been built up and is unique in the field of large engine and SCR testing systems.

In order to provide an additional degree of freedom with regard to parameter for the engine operation optimization an additional adapted control system ("Intelligent SCR" control) has been specified. During the project, the control system has been designed and installed at the engine. After commissioning the installation will be utilized for the technology development and enables the possibility to further increase the performance of the system.



2.2 Description of the exhaust gas after treatment system

The SCR reactor is a combiKat© compact SCR System (Anlage Nr. 5144) with a combiKat© Reaktor EM40/6 (Figure 3) and a SNQ NO_x-Controller that was commissioned in 2009 by Hug Engineering AG.

In the framework of this project, various updates and changes were implemented (see Figure 4 and Figure 5):

Mass flow was optimized using CFD to achieve an uniformity index higher than 99%

- Dosing element was replaced by a high-end mass flow controller with minimum retention time
- Catalysts were replaced with RFV.C5 with a pitch of 103 cpsi in order to minimize the catalyst volume and thus increase the system reaction time.
- Approx. 30 thermocouples were installed for mapping out the temperature within the entire catalyst volume
- FTIR up and downstream are available
- NO_x Sensor up and downstream are installed
- NH₃ Sensor downstream is installed



Figure 3: combiKat© compact SCR reactor from Hug Engineering, located at the LERF facility

The reduced catalyst volume as well as the updated dosing system and flow uniformity were achieved for making the entire system prepared for the higher performance demands in this project. The updated system allows one to track and fully capture quick variations such as step responses from load changes or transient load following.

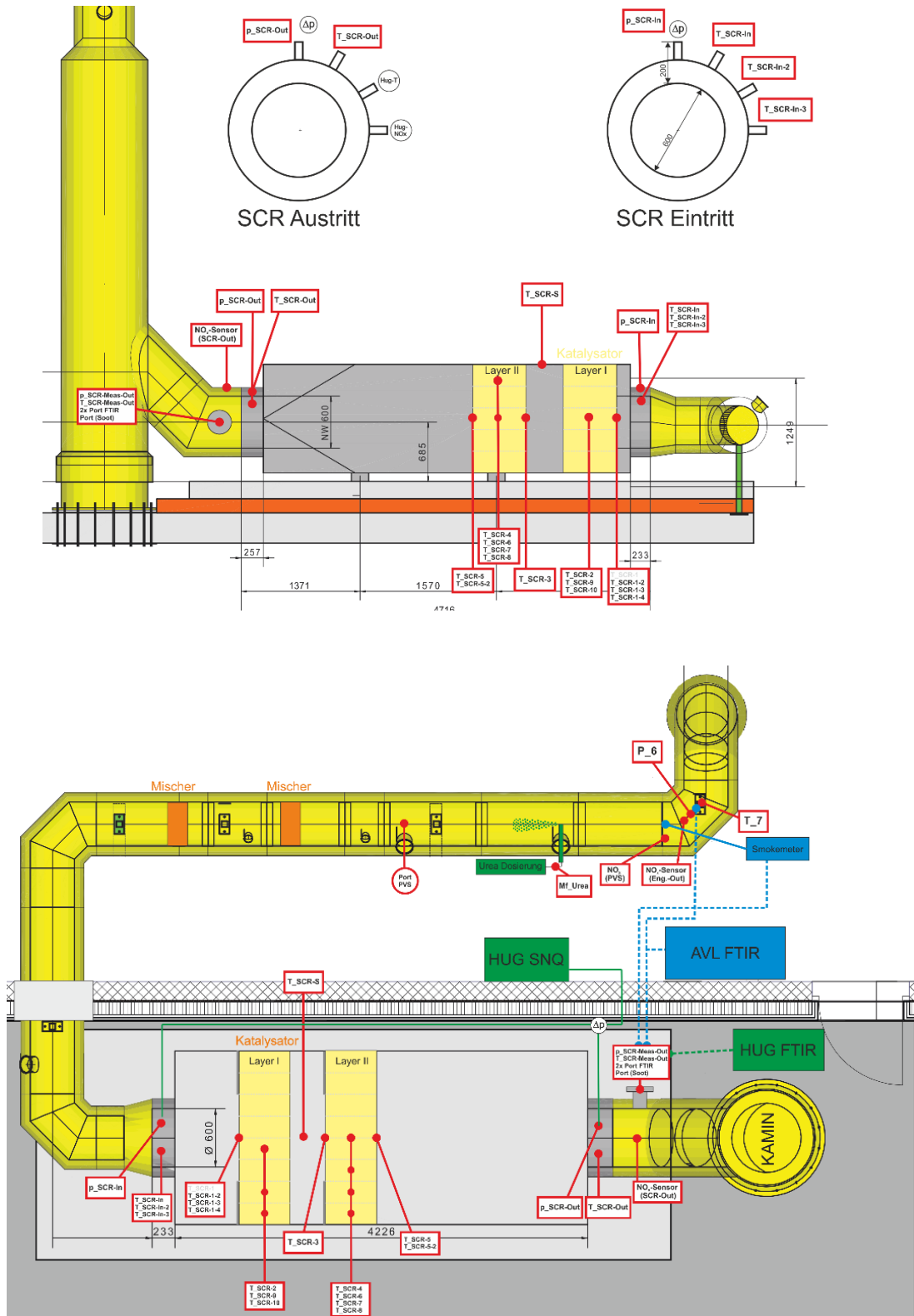


Figure 4: Design of the exhaust gas after treatment system installed at the LERF facility after implementation of the updates mentioned above (top: side view, bottom: top view).

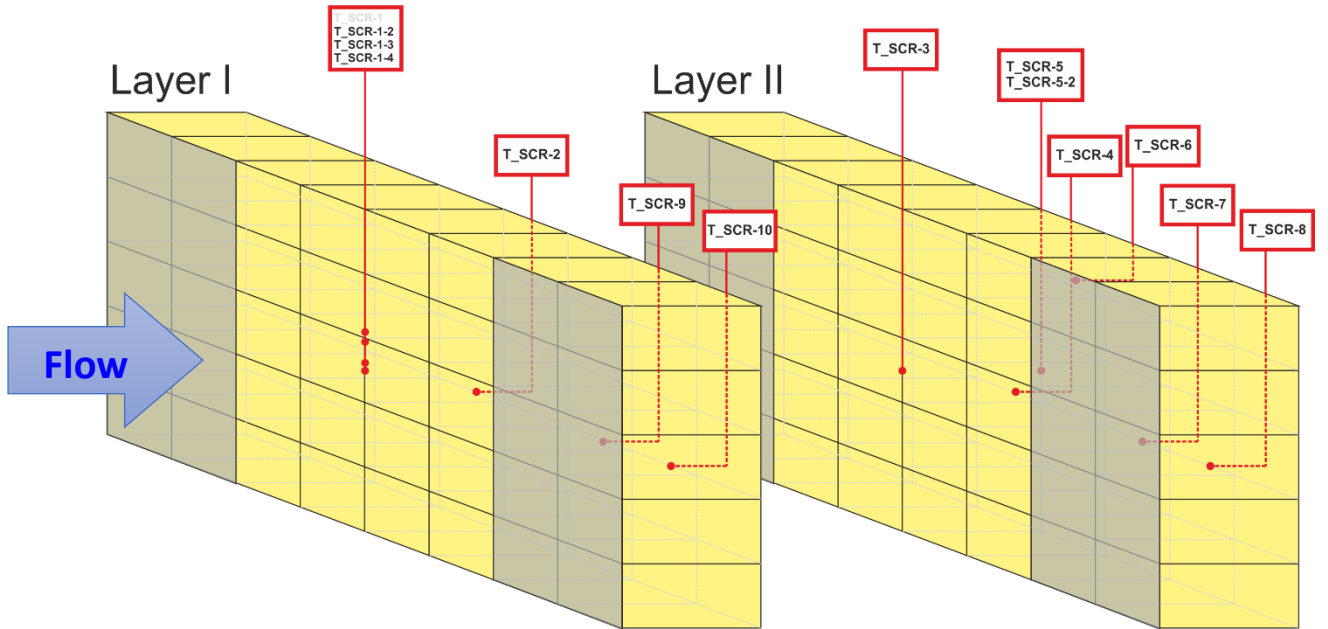


Figure 5: Temperature sensor installations throughout the two catalyst layers



3 Procedures and methodology

3.1 Description of the test cycle

In order to test all different control strategies in a comparable way, the project team has defined a comprehensive test cycle (see Figure 6). It is programmed with the AVL test facility control system and defines the desired speed, torques and waste gate position at various load points. The cycle runs automatically and with the additional data system installed, all necessary information/measurements can be observed and recorded.

At the beginning, the engine ramps up to 10% load in order to check all components and systems to ensure their proper operation. Afterwards, the engine ramps up to 90% load (100% load is avoided due to lack of flexibility of control parameter adjustment as some safety constrains like high temperatures etc. are within easy reach). During the load increase, also the waste gate is opened to the desired position: 25% between 10 and 75% load and 33% above 75% load. After that start-up phase, stationary load points are set in order to have stable conditions that are also a reference to very other testing day.

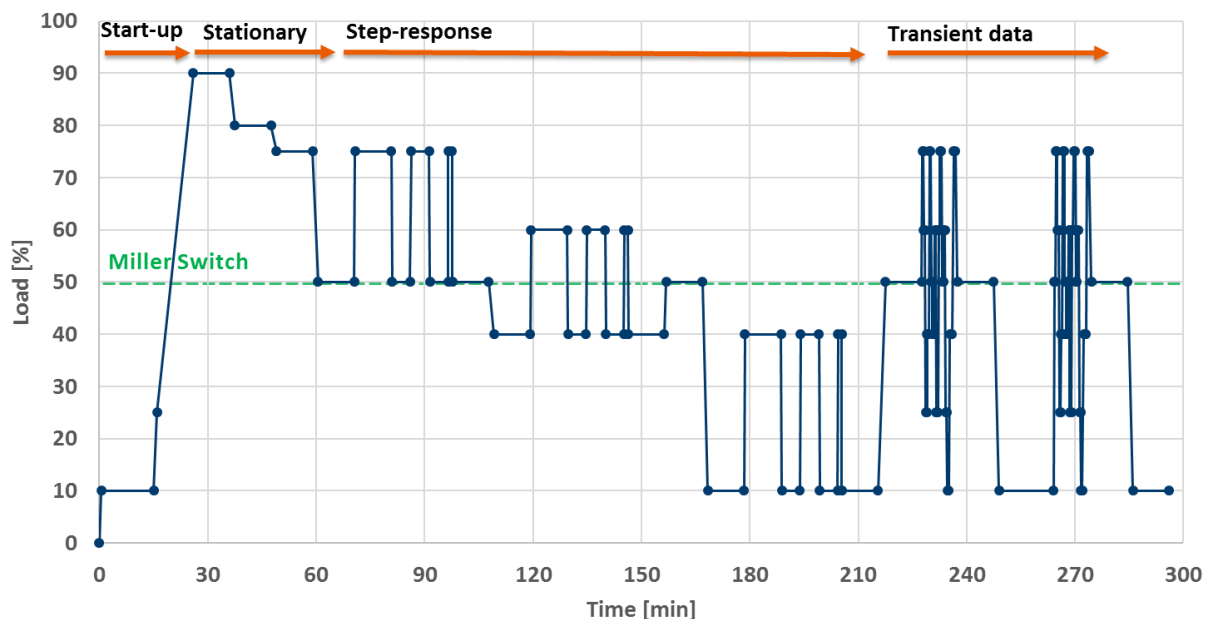


Figure 6: Overview of the specially defined engine test cycle for the "intelligent" SCR project

In a next stage, the cycle includes step-responses with regard to NO_x freight changes for the SCR. There are three load changes where each of them has three load and deloading ramps with different ramping times: 50 to 75%, 40 to 60% (including miller time change) and 10% 40% load. At these load changes are also different temperature levels present, beside the variation of NO_x . These load changes are also a prerequisite for the modelling task within this project. The defined step-responses, starting from very comparable engine conditions, are inevitable for the development of NH_3 storage and conversion models. Figure 7 shows a detailed extract of step-responses 50 to 75% load from the overall test cycle.

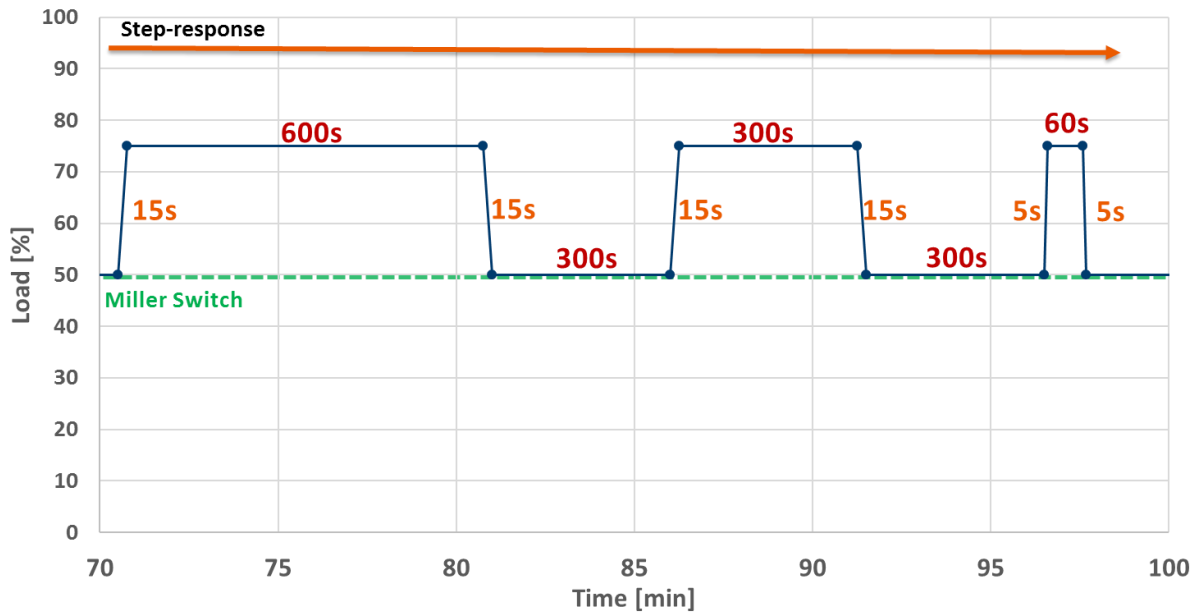


Figure 7: Extract from the overall test cycle showing the step-response ramps and holding times of the 50-75% load changes

Finally, the test cycle includes a transient stage in order to evaluate the performance of the SCR systems at non-stationary conditions, which occur during manoeuvring or position holding operation of vessels as well as load following procedures for stationary engines systems (see Figure 8). Preliminary tests have shown that the starting load and hence, the corresponding temperature/ NO_x levels do have a significant influence (history effect) along the defined transient cycle. Therefore, the transient load changes are starting from 50% and 10% load to assess this effect as well.

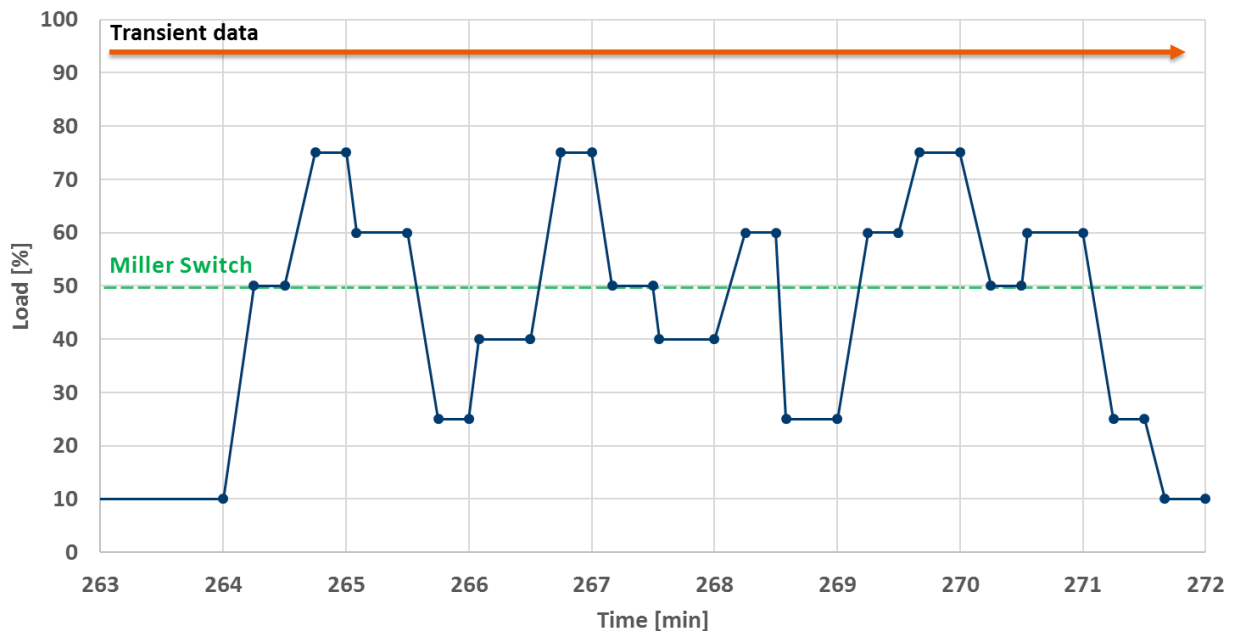


Figure 8: Transient stage of the test cycle starting with 10% load



3.2 Description of the SCR control strategies

In the project, several control strategies were defined in order to steadily increase the complexity of the system. In Table 2, all the control strategies are listed together with the tools needed as well as the current status. For all strategies, the identical cycle, explained above, is used in order to make the results comparable.

Table 2: Control strategies used in this project, listed with increasing complexity

Control strategy	Abbr.	Necessary tools	Testbench
Static dosing table	<i>DT-0.9</i>	- Engine NO _x out map	Real
Feed Forward	<i>FF-0.9</i>	- NO _x Sensor upstream	Real
	<i>FF-0.95</i>		Virtual
Feed Forward PVS	<i>FF-PVS-0.9</i>	- NO _x Freight from PVS	Real
Offline optimized	<i>Off Opt</i>	- Optimization algorithm	Virtual
		- Static SCR model	Real
Hybrid optimized	<i>Hyb Opt</i>	- Optimization algorithm	Virtual
		- Dynamic SCR model	Real
Online optimized	<i>On Opt</i>	- Online optimization algorithm - dynamic SCR model - Peak pressure and temperature controller	Virtual

For the control strategy *DT*, a urea water dosing table (Table 3) based on a measured engine NO_x map was implemented. The engine NO_x map was established prior to the *DT* measurement campaign.

Table 3: Engine NO_x Map and corresponding urea dosing amounts for alpha 0.9

Engine load	[%]	100	80	75	50	48	25	10
NO _x freight	[mol/h]	184	197	132	76	164	81	65
Urea water [40%]	[L/h]	10.7	11.45	8	4.5	10.5	5	4.1

For the control strategy *FF* and *FF-PVS*, a simple control concept was implemented in the software environment of the system. The NH₃ dosing was calculated either from the exhaust gas mass flow and the NO_x concentration from the Sensor (*FF*) or from the NO_x freight provided by the PVS system (*FF-PVS*). The desired alpha (NH₃/NO ratio) was set to 0.9, identical to the one from control strategy *DT*, and to 0.95, for *FF-0.9* / *FF-PVS-0.9* and *FF-0.95* respectively.

In the optimized control strategies (*Off Opt*, *Hyb Opt* and *On Opt*), the engine and catalyst setup are optimized either offline, combined offline and online (Hybrid) or online. In the *Off Opt*, the engine settings



(SOI and WG) and urea dosing are optimized at steady state engine operation using a virtual testbed (described in detail in section 3.4) in order to minimize fuel consumption and simultaneously NO_x and NH_3 emissions. The hybrid optimization also includes an urea injection rate adapted online using information from the catalyst state in real time. This measure is taken in order to reduce NH_3 slip and/or NO_x emissions during transients. Both *Off Opt* and *Hyb Opt* cycles have been tested on the testbench; the results for these cycles can be found in the results section of this report (Section 0).

The *On Opt* cycle includes a coupled online optimization of the SOI, WG and urea dosing in order to further improve fuel consumption and emissions during transients. This final cycle has only been tested using the virtual testbench. The results of the optimization are provided in the outlook (Section 6).

The contribution of Vir2sense to this research project is the prediction of the correct engine settings to emit the desired engine out NO_x under the constraint of the best achievable fuel consumption. For this purpose, the Physically-assisted Virtual Sensor (PVS) has been installed. The PVS is a prototype device which combines combustion and emission model calculations and measurements to recalibrate and adapt the model outputs without human intervention (Figure 9). In a first step, the PVS prototype is modified until the output signal quality level is sufficient for SCR control. In a second step, the SCR is controlled only by the PVS signals and compared to the other strategies.

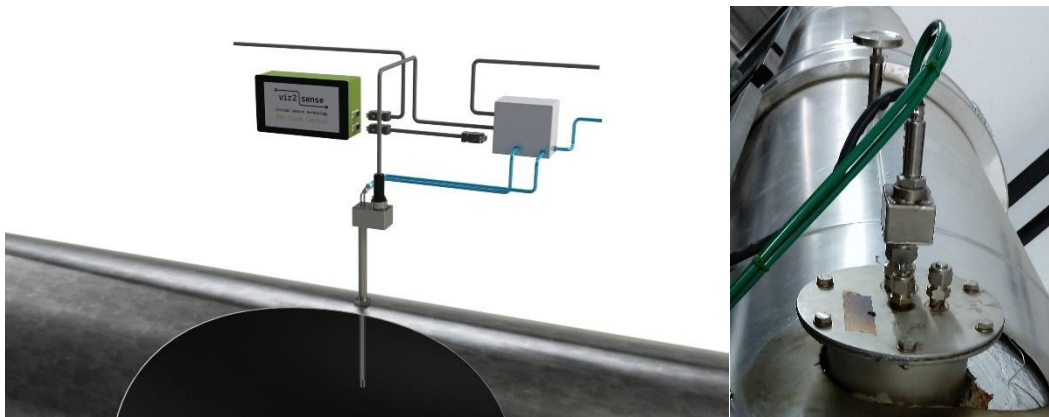


Figure 9: PVS Prototype



3.3 SCR Model

Modelling

In order to predict NO_x and NH₃ clean gas emissions in relation to engine out emissions and operation conditions, a model of the SCR catalyst is required. The model represents a 1D finite element representation of the catalyst, meaning that each catalyst layer is represented by 10 cells of equal length covering the whole cross-section. Each of these cells has three internal states (temperature and two NH₃ storage levels). The NH₃ storage is required as only NH₃ stored on the catalyst is able to take part in the SCR reaction. However, it has been shown that models with a single storage model are unable to properly describe NH₃ slip. Therefore, a secondary storage has been included into the model. While for both NH₃ storage parts, there are adsorption and desorption rates, all modelled chemical reactions (SCR and oxidation) are only included in the primary storage model. The temperature of each catalyst cell is determined by means of an energy balance including the heats of reaction.

In conclusion this results in three differential equations which, for each cell, are integrated over time:

$$\frac{d\theta_A}{dt} = \frac{1}{m_{\text{cell}}c_{S,A}} \left(R_{\text{ads}}^A(c_{\text{NH}_3}, \theta_A, T_{\text{cell}}) - R_{\text{des}}^A(\theta_A, T_{\text{cell}}) - R_{\text{SCR}}(c_{\text{NO}}, \theta_A, T_{\text{cell}}) - R_{\text{oxi}}(\theta_A, T_{\text{cell}}) \right)$$

$$\frac{d\theta_B}{dt} = \frac{1}{m_{\text{cell}}c_{S,B}} \left(R_{\text{ads}}^B(c_{\text{NH}_3}, \theta_A, T_{\text{cell}}) - R_{\text{des}}^B(\theta_A, T_{\text{cell}}) \right)$$

$$\frac{dT_{\text{cell}}}{dt} = \frac{1}{m_{\text{cell}}c_{\text{cat}}} \left(\dot{Q}_{\text{conv}}(\dot{m}_{\text{ex}}, T_{\text{ex}}) + H_{R,\text{SCR}}(R_{\text{SCR}}) + H_{R,\text{oxi}}(R_{\text{oxi}}) \right)$$

with θ_A , the primary NH₃ storage, θ_B the secondary NH₃ storage, T_{cell} the catalyst temperature, R_{ads}^* the adsorption rate into storage *, R_{des}^* the desorption rate from storage *, R_{SCR} SCR reaction rate, R_{oxi} the NH₃ oxidation rate, \dot{Q}_{conv} convection heat transfer from the gas phase to the catalyst, $H_{R,*}$ enthalpy of reaction (SCR or NH₃ oxidation), c_{NH_3} concentration of NH₃ within the gas phase, c_{NO} concentration of NO within the gas phase, m_{cell} catalyst mass within each cell, $c_{S,*}$ NH₃ storage capacity of storage *, c_{cat} catalyst heat capacity, \dot{m}_{ex} the exhaust gas mass flow and T_{ex} the exhaust gas temperature.

In order to determine the parameters of the first two equations a number of laboratory experiments were conducted (Figure 10). The parameter for the heat transfer equation can only be determined based on test runs on the testbench.

Reaction Kinetics Experiments – Setup

The experiments for the reaction kinetics were designed and performed at PSI within the group of “Applied Catalysis and Spectroscopy“ in collaboration with Hug Engineering. The catalysts used in the experiments were provided by Hug Engineering. The main goal of the experiments was to generate a complete dataset to establish the abovementioned SCR model as well as to verify the model parameters.

A scheme of the laboratory test rig at PSI is presented in Figure 10. The main parameters of the tests were the following:

- General gas composition: 5 vol% H₂O, 10 % O₂ in N₂.
- Mass flow: 450 – 700 IN/h (SV-dependent)
- Catalyst volume: 20 – 40 cm³ (SV-dependent)
- Catalyst: Fully extruded V-based SCR catalyst - 100 cpsi

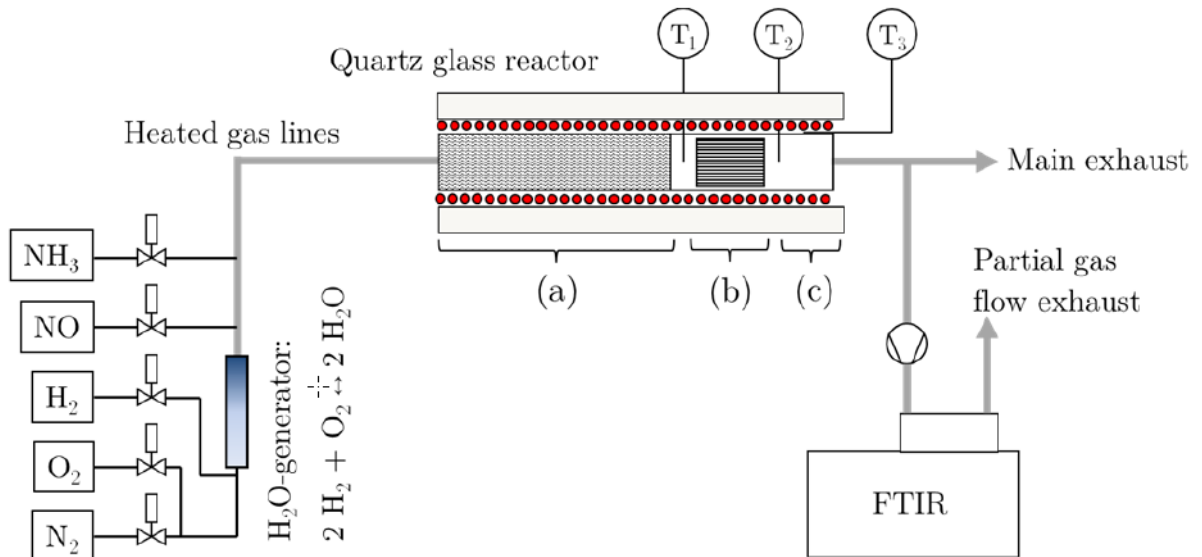


Figure 10: Laboratory test rig with a gas mixing set up, heated gas lines, H₂O generator, quartz glass reactor and a FT-IR spectrometer. To ensure uniform temperature along the reactor bed, the reactor was divided into three heating zones: (a) preheating with ceramic beads and temperature control at T₁, (b) length of the catalyst bed with the temperature control at T₂ in the center of the reactor and (c) reactor outlet the temperature control at T₃. A partial gas flow was actively let through the gas analysis, a Fourier transform infrared spectrometer with a 2.0 m gas cell.

3.3.3

Reaction Kinetics Experiments - Measurement

- a) Steady state experiments (Equilibrium measurements)
 - a. Three different GHSV (12'000 h⁻¹ and 16'000 h⁻¹ and 24'000 h⁻¹)
 - b. Temperatures: 500°C, 450°C, 400°C, 350°C, 300°C and 250°C
 - c. Three different NO concentrations (300, 500 and 1000 ppm)
- b) Dynamic experiments (rapid dosage changes)
 - a. Three different GHSV (12'000 h⁻¹ and 16'000 h⁻¹ and 24'000 h⁻¹)
 - b. Temperatures: 500°C, 450°C, 400°C, 350°C, 300°C and 250°C
 - c. Two different NO concentrations
- c) Temperature ramps (250 – 450°C, 20-30°C/min)
 - a. Three different NH₃ dosing (o.D.= alpha at 10ppm NH₃ slip; 0.8*oD; 1.2 *oD)
 - b. Two different NO concentrations
 - c. Three different GHSV (12'000 h⁻¹ and 16'000 h⁻¹ and 24'000 h⁻¹)
- d) Periodically empty pipe measurements without catalysts (Benchmarking & Threshold)



Reaction Kinetics Experiments – general procedure

a) Steady state experiments (Equilibrium measurements)

The general procedure for steady state experiments are listed below. In Figure 11, the procedure is shown as an example.

3.3.4

- I. At constant temperature and 700 ppm NO dosage search for alpha o.D. by changing NH₃ dosage (= alpha optimal dosage → alpha corresponding to 10 ppm NH₃ slip; ±1 ppm)
- II. Operate without NH₃, only with 700 pm NO catalyst.
- III. One after the other alpha o.D, alpha o.D.*0.8 and alpha o.D.*1.2, wait for equilibrium
- IV. NH₃ storage without NO metering: Completely remove NH₃ from the catalyst with NO metering, stop NO metering. Dose 700 ppm NH₃ and wait for equilibrium.
- V. Stop the NH₃ dosing. Depending on the desorption behavior, titrate the remaining NH₃ with NO.

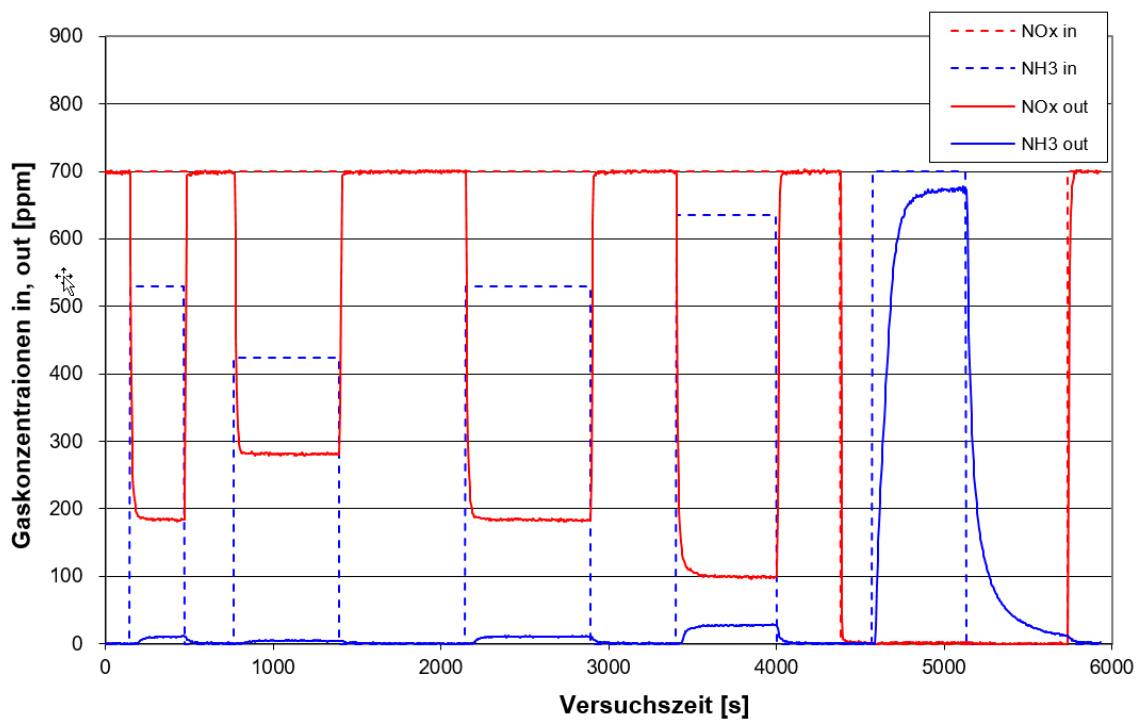


Figure 11: Example of a steady state experiment (equilibrium measurements) performed for the SCR parameterization



b) Dynamic experiments (rapid dosage changes)

The general procedure for dynamic experiments is listed below. In Figure 12, the procedure is shown as an example. The dosage changes were made using an automated time program.

- I. Constant temperatures and 700 ppm NO dosage with dosage change $\alpha \text{ o.D} \times 0.8$; $\alpha \text{ o.D}$ and $\alpha \text{ o.D} \times 1.2$.
- II. Starting with $\alpha \text{ o.D} \times 0.8$, 2 x in succession 30 s, 60 s, 120 s, 240 s and 480 s NH₃ dosing on and the same pulse length NH₃ dosing off in between.
- III. Then the same pulses with the other two α values.

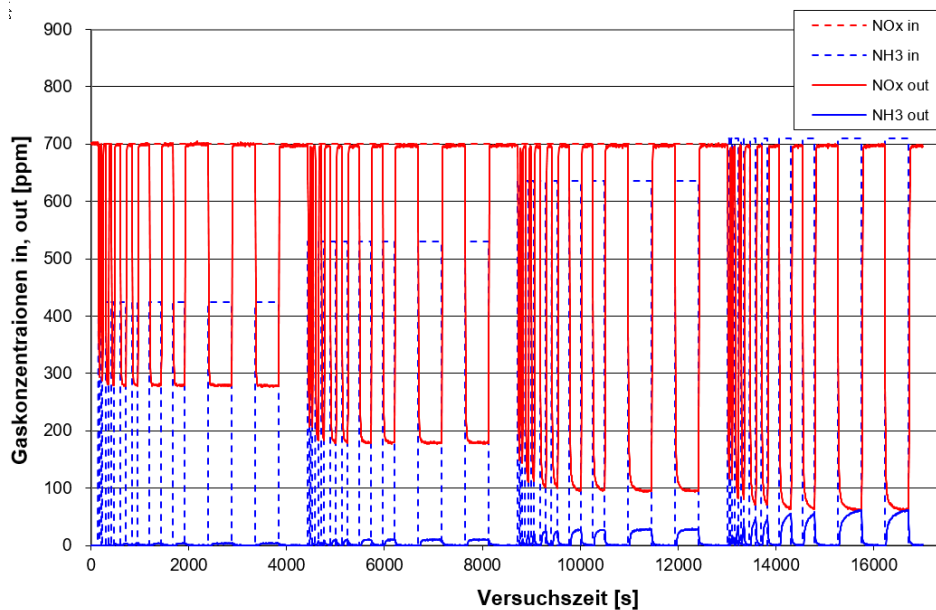


Figure 12: Example of a dynamic experiment performed for the SCR parameterization.

3.3.5

Parameter Determination

The results from the laboratory experiments were subsequently used to determine the model parameters. This was achieved by numerical optimization of the model parameters. Thereby all parameters of the SCR model related to reaction kinetics as well as their dependence on temperature have been determined.



3.4 Optimization procedure

Engine optimization includes a wide field of opportunities and measures and optimization criteria. In the present case, the optimization criteria are fuel consumption, tail pipe NO_x emissions (after catalyst) and ammonia slip. The engine parameters to be adjusted are start of injection (SOI), waste gate (WG) and urea (ammonia solution) dosing. In order to find the best engine parameter configuration for the actual load requirements, the effect of each combination needs to be known for each engine load. This relationship can either be extrapolated from a series of measurements or obtained using a calibrated model. The quality of the first option depends on the number of measurement points, while the quality of the second from the model predictability. Due to limited testbench accessibility in the current pandemic situation, a virtual full engine testbench has been developed and consequently used to serve with the data for the engine operation optimization. The following section describes the architecture of a virtual testbench and the optimization procedure.

Virtual engine testbench

The virtual testbench contains a similar cylinder model (compression, combustion, emissions and expansion) as the PVS, with additional modeling of the full gas exchange process. In order to run these submodels without the inputs of the real engine, a turbocharger and air path model and a load controller have to be added. In addition, to judge the tail pipe emissions, an SCR model is required as well. The operating condition set points as SOI, fuel pressure, load demand and WG position are adjustable in a virtual electronic control unit (ECU). Figure 13 shows an overview of the virtual testbench with all its components.

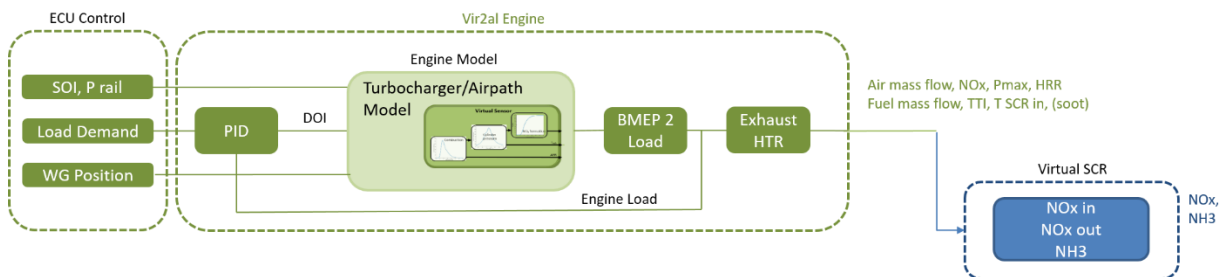


Figure 13: Schematic view of virtual testbench

3.4.2

Engine operation optimization:

The target of the engine operation optimization is a minimized fuel consumption under given constrains, which are tailpipe NO_x and NH₃ emissions, peak cylinder pressure and exhaust gas temperature. The engine settings to be changed are start of injection, waste gate position and urea dosing. To choose the best settings combination, it is crucial to know the outcome of the quantities to be optimized for each combination at each engine load. However, not all quantities are directly available. For example, the tailpipe NO_x needs to be calculated using the exhaust NO_x and the expected SCR conversion efficiency. The conversion efficiency itself is a function of temperature and space velocity. Therefore, maps for SCR temperature and space velocity need to be available. Figure 14 demonstrate this process. The top left map shows the relationship between SCR conversion efficiency, space velocity (reciprocal gas residence time) and temperature at a constant ammonia slip (here 10 ppm). These values are characteristic for a certain catalyst. In the present case, the values have been obtained through the SCR model. The bottom left and right map serve with the space velocity and the temperature respectively for a variation in SOI and WG at 70% load. With these three maps, conversion efficiency maps as a function of SOI



and WG can be constructed for each load. Similar maps need to be calculated for exhaust NO_x freight, peak pressure, maximum exhaust temperature and brake specific fuel consumption. The brake specific fuel consumption map now needs to be restricted to areas where the peak pressure, the maximum exhaust temperature and the constrained tailpipe NO_x emissions. The latter are calculated using the exhaust NO_x freight map and the conversion efficiency map. Figure 15 shows the map of brake specific fuel consumption at 70% load for all SOI and WG combinations which do not exceed the peak pressure, the maximum exhaust gas temperature or the desired tailpipe NO_x freight, which was here chosen to be 10% of the exhaust NO_x freight with the initial (reference) engine setup. This provides an abatement of 90% of the reference.

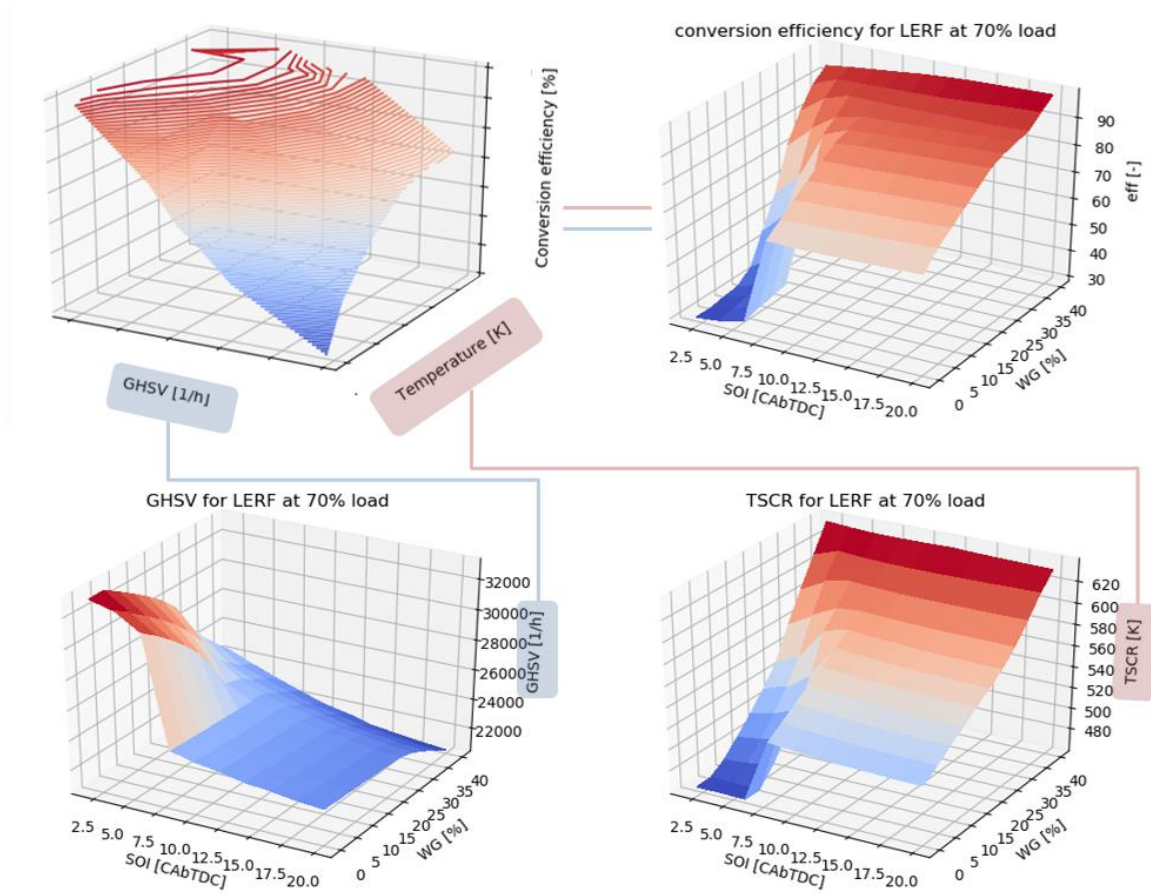


Figure 14: Demonstration of the construction of a conversion efficiency map (top right) using the gaseous hour space velocity (bottom left), the SCR temperature (bottom right) and the SCR conversion characteristic map (top left).

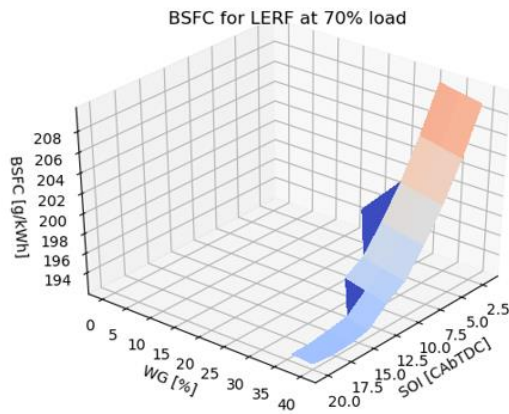


Figure 15: BSFC map at 70% load for a reference abatement of 90%.

In order to enable a flexible optimization, the calculation has not only been performed for 90% reference abatement but also for other percentages. Figure 16 shows the resulting maps for SOI and WG settings for all loads and a variation of reference abatement. The reference abatement represents the tailpipe NO_x limit. For the present project, the NO_x limit is expressed as a percentage of the exhaust NO_x emissions under reference SOI and WG settings. This has the consequence, that the effective abatement can be different to the reference abatement as soon as the exhaust NO_x values are different. The figure indicates the reference abatement of 0.9 with a red line. This is the target line to meet similar tail pipe NO_x emissions as in the reference cycle with the least possible fuel consumption. The tail pipe NO_x limit can also be expressed as an absolute value instead of a reference abatement. For higher reference abatements, the engine settings change towards higher fuel consumption. Below a reference abatement of 0.88, the engine settings do not change further, which means that NO_x is not a limiting factor anymore. Some load conditions (e.g. 30 %) also allow higher NO_x abatement without a penalty in fuel consumption (but with increased urea consumption, which has not been weighted in the present work).

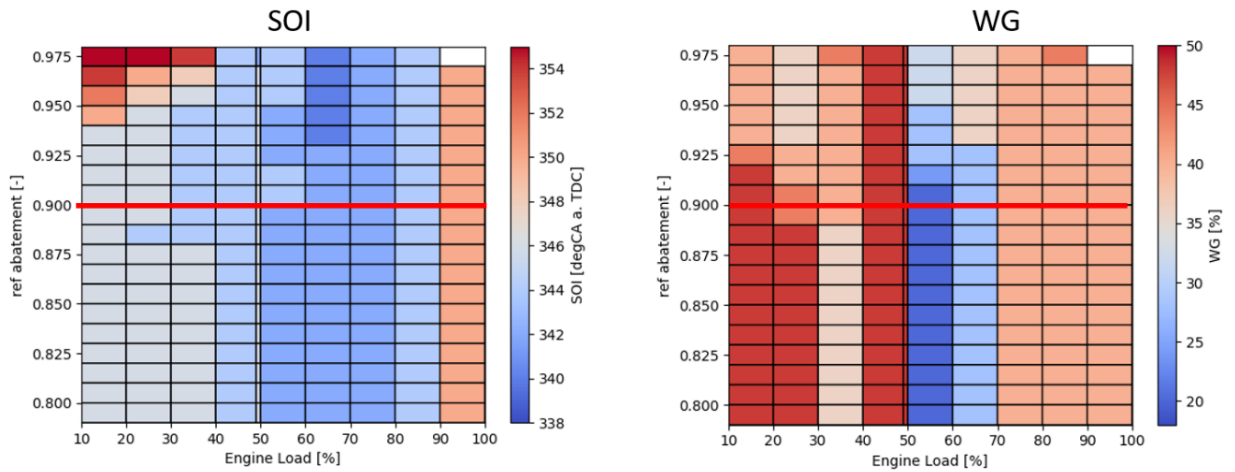


Figure 16: SOI (left) and WG map for all engine loads and a wide range of reference abatements.

The corresponding urea consumption, and thus the effective abatement, are calculated from the NO_x conversion map. Figure 17 shows the effective target abatement (or alpha, the ammonia to NO_x ratio, normalized with the stoichiometric ratio). As abovementioned, the values are typically higher than the reference abatement for two reasons: First, the engine setup allows higher abatement without penalty in fuel consumption. Second, the change in SOI and WG in contrast to the reference conditions increase exhaust NO_x, which requires a higher abatement to achieve the target tailpipe NO_x.

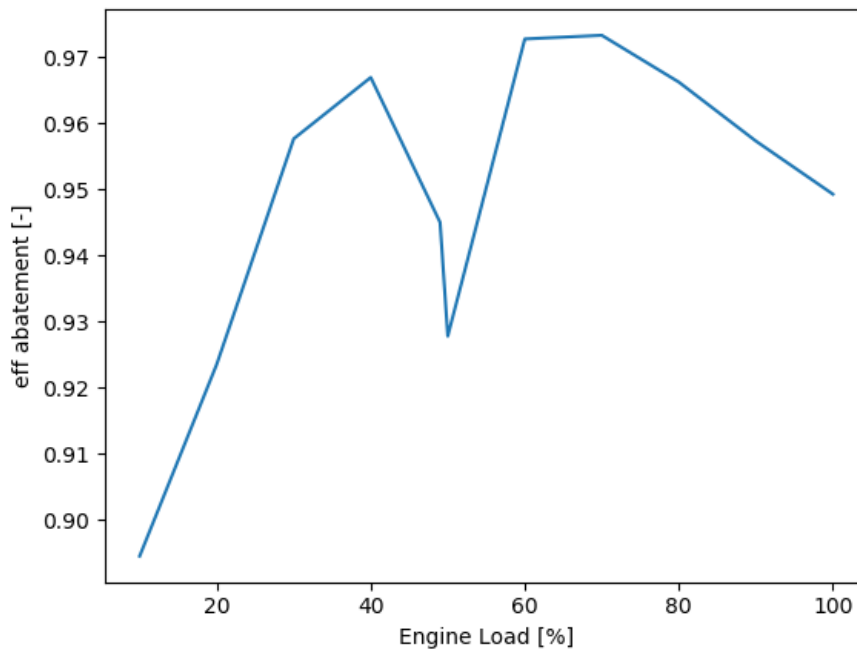


Figure 17: Effective abatement for reference abatement of 0.9.



Once this setup was established using the virtual testbed, it could be loaded directly on the engine (SOI and WG) and catalyst ECU (target effective abatement respectively alpha); this setup is labelled offline optimization (*Off Opt*). In order to overcome the fact that the engine is not always operated under steady state conditions and does not always see similar environmental conditions, the offline optimization has been further adapted to operate online.

The benefit of the online optimization lies in the possibility to include the actual catalyst status by means of ammonia storage and temperature to either adapt the engine settings (SOI and WG) or the requested urea. This is important due to the high thermal inertia of the catalyst. In addition, the exhaust NO_x for all SOI and WG settings is a key input to calculate the optimum engine settings. With online-performed optimization, the maps used can be adapted to account for environmental impact on NO_x emissions. The correction factors can be found from the actual PVS calibration. Furthermore, an active peak pressure and exhaust temperature limiter can be directly included in the algorithm to avoid engine operation limits during transient operation. The first of the three mentioned opportunities has been realized by implementing the SCR model into the online optimization to be operated as an SCR digital twin. The second has been realized by transferring the change in NO_x model parameters from the PVS to account for changes in model calibration during operation. This way, also the online optimizer accounts for changes outside of the NO_x model inputs (e.g. component ageing or fuel composition changes). The last of the three opportunities have been realized with two separate, adapted PID controllers to limit the peak pressure and exhaust temperature in transient operating conditions where the steady state air path parameter like intake manifold pressure are different to the actual (mainly due to thermal and mass inertia of the turbocharger). The online optimizer has been compiled to an executable, which operates on one of the testbench computers and uses an OPC interface to communicate with the engine and the PVS. The settings of the online optimizer can be controlled with GUI as displayed in Figure 18.

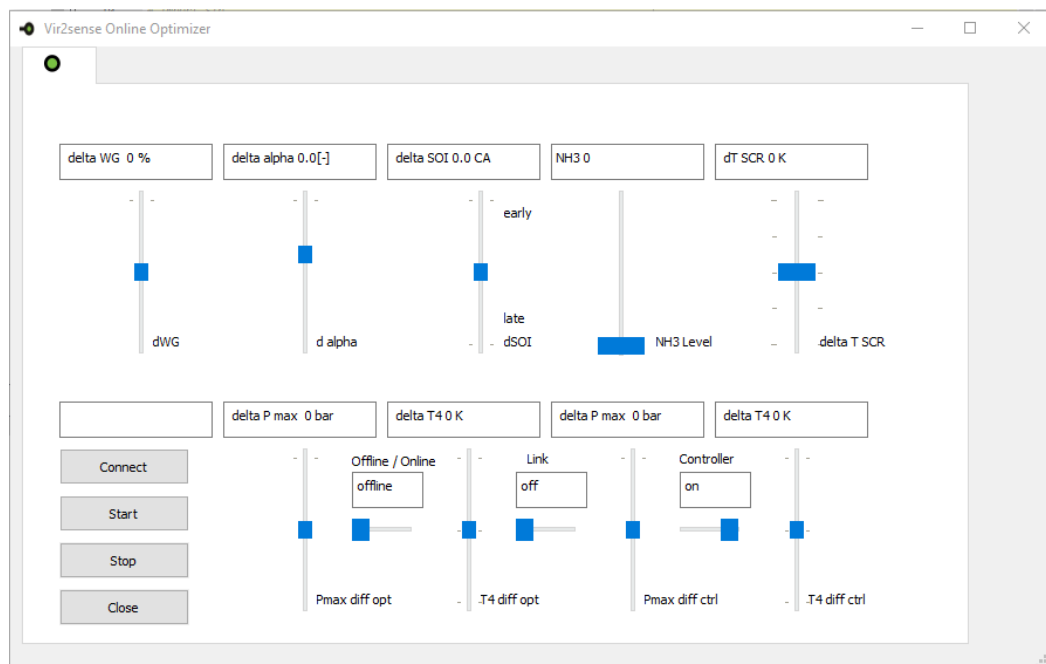


Figure 18: GUI for online optimizer.



The online optimizer has the ability to directly influence SOI, WG and alpha. It displays the catalyst ammonia storage level and the catalyst internal temperature difference in comparison to the gas temperature at SCR inlet. The peak pressure and temperature limits can be changed for the optimization and for the peak pressure and temperature limiter (separately or linked). The peak pressure and limiter can be switched on or off. The optimization can be performed online, which requires engine ECU access to modify SOI and WG online or offline, where the digital twin of the catalyst only affects the urea dosing. In the latter, only the map of SOI and WG need to be modified.

In order to test all variants of algorithms with the limited access to the testbench, the PVS and the online optimizer have been adapted to operate with the virtual engine. The virtual engine setup is visible in Figure 19.

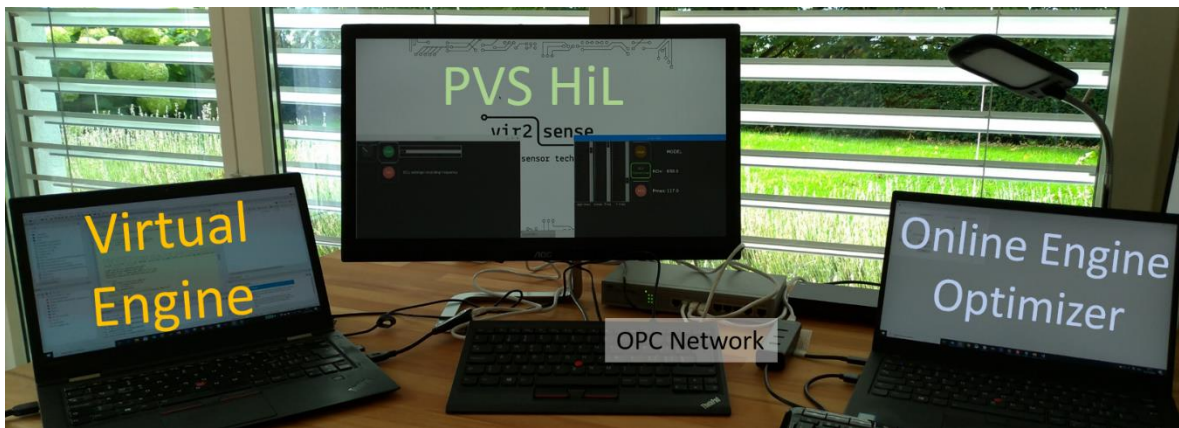


Figure 19: The virtual testbench environment with the virtual engine including SCR (left), the PVS hardware in the loop (HiL, center) and the online engine optimizer (right), connected through an OPC network.



4 Results and discussion

4.1 SCR model

Model parameters

4.1.1 The group of applied catalysis and spectroscopy at PSI has provided the entire data set for the current installed SCR catalyst. The dataset is complete and consistent. Specific datapoints cannot be discussed in this report because the data could reveal sensitive information about the catalyst performance. The data is directly used to set up and optimize the SCR model.

SCR modelling

4.1.2 There are two ways to assess the performance of the SCR model: Firstly, a comparison between the laboratory data and the model prediction and secondly, a comparison between testbench data and the model. As the first comparison is based on the same data as the parameter fitting, only limited information on the prediction power of the model can be obtained. However, this comparison is important to judge the quality of the parameter fitting. As no testbench data has been involved in the fitting of the reaction parameters, a comparison between the testbench data and the model allows to judge the ability of the model to predict the performance of the SCR under working conditions.

In Figure 20 the comparison between the model and the laboratory data ($T=3350^{\circ}\text{C}$, $V=635\text{NI/h}$) is shown. As expected, the model is able to predict the results with minor differences.

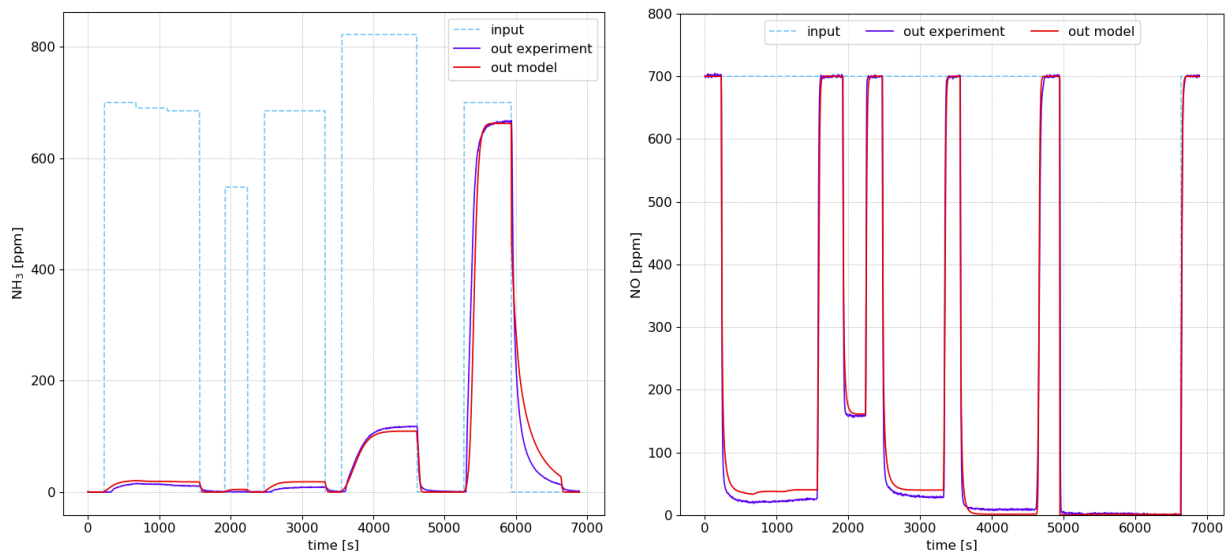


Figure 20: Comparison between experimental data and the model prediction at 350°C and 635 NI/h

More interesting is the comparison shown in Figure 21. Therein the clean gas NH_3 emissions of a full cycle on the test bench is compared to the model prediction. As it can be seen, the model doesn't fit as nicely as before. But nonetheless, it is easily able to predict all the trends. NH_3 emissions are notoriously difficult to measure both accurately and fast. Therefore, for this comparison the values obtained by a



NH₃ sensor are taken into account. This sensor has a relatively high measurement error but is significantly faster than the more accurate FTIR readings. Thereby, fluctuations in NH₃ emissions during transient operations are much better covered. Judging from this comparison one of the main issues of the model is related to steps from low temperatures to high. As stated before the model is able to predict an increase in NH₃ emissions, but the magnitude is consistently underestimated.

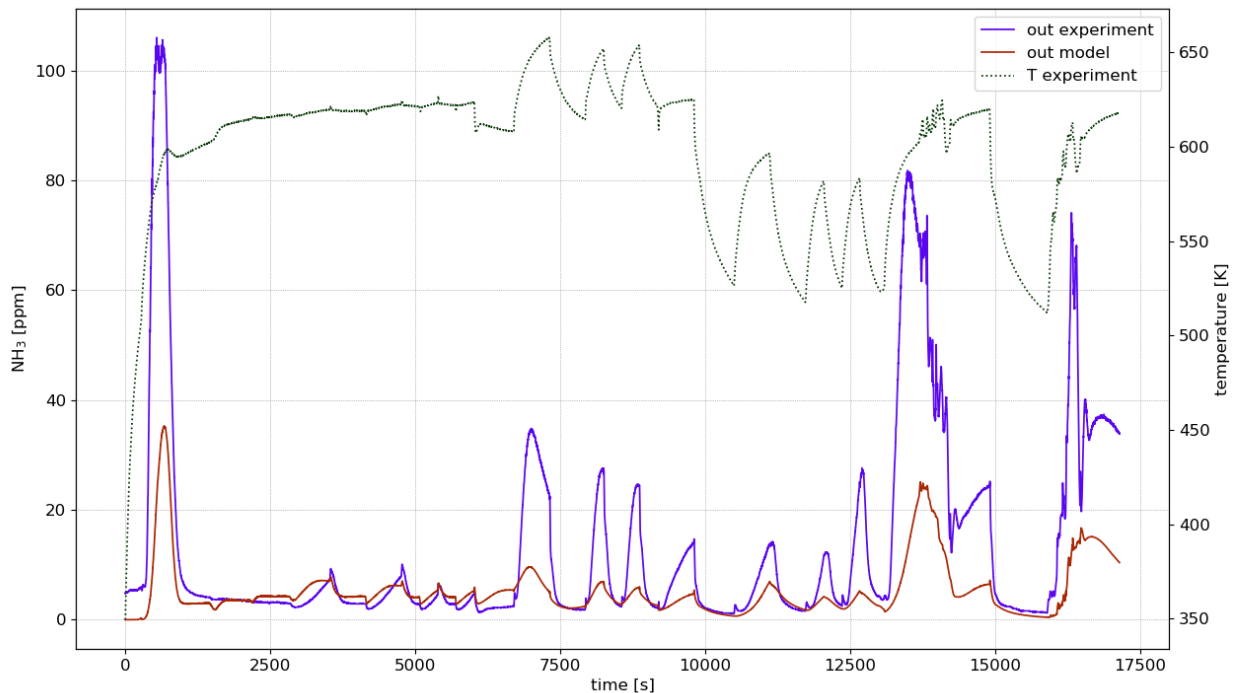


Figure 21: Comparison of NH₃ slip between LERF test run and the SCR model, taking into account the influence of exhaust gas temperature.

4.2 Virtual Testbench

Figure 22 shows a comparison of the measured load and injection duration (DOI) and the respective outputs from the virtual testbench. The performance of the virtual ECU and the load controller is very good and the measured engine load can be matched with a very similar but smoother DOI. The sampling frequency of the measurement data acquisition is one second. The calculation duration of one cycle is depending on the load demand, but on average it is around 200 ms. Therefore, a full cycle simulation is approximately five times faster than real time.

Figure 23 compares the measured exhaust and tailpipe NO_x emissions with the corresponding modelled values. The accuracy of both the exhaust (before SCR) and the tailpipe emissions is high. Only at operating conditions with 10% load, the model underestimates the exhaust emissions. However, the NO_x freight at these points is low, and therefore, the error does not weigh high in the cumulative NO_x mass calculation. Additionally, the prediction of the tailpipe NO_x also shows a high accuracy.

Another important quantity to enable an engine operation optimization is the SCR temperature, since this temperature strongly influences the predicted NO_x reduction ability of the catalyst. A comparison of the measured and modelled SCR temperature is depicted in Figure 24.

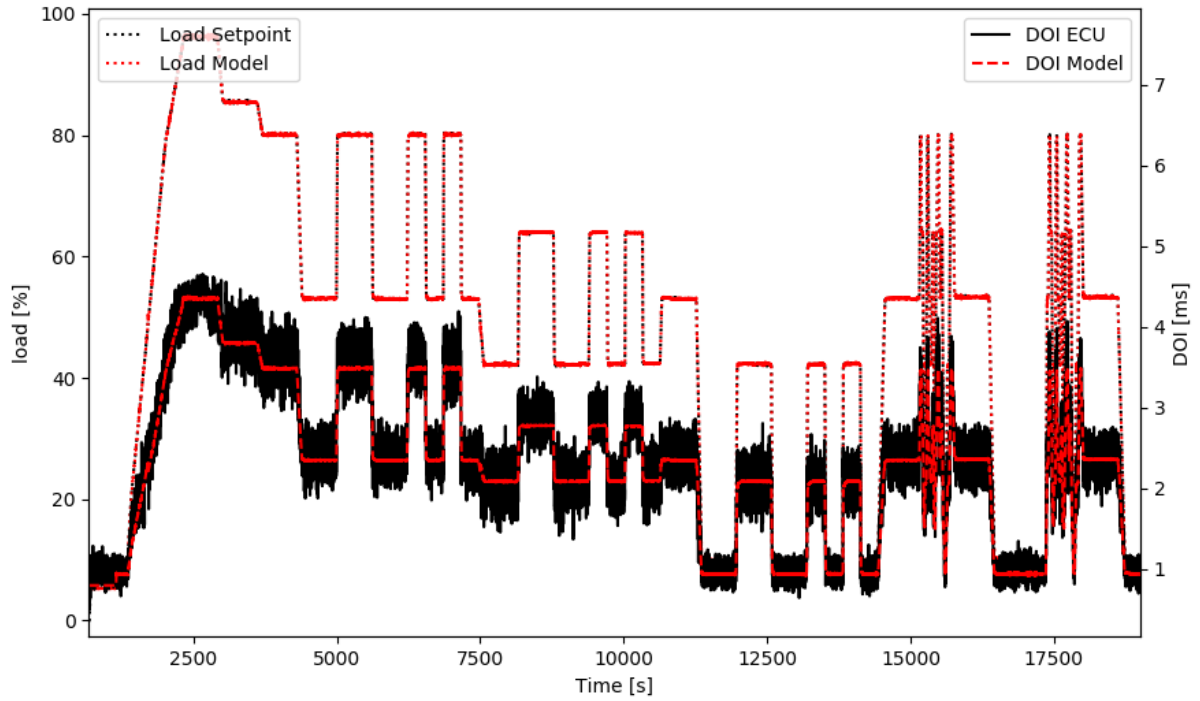


Figure 22: Engine load (left) and DOI during the test cycle. Measured values (black) versus values from the virtual testbench (red).

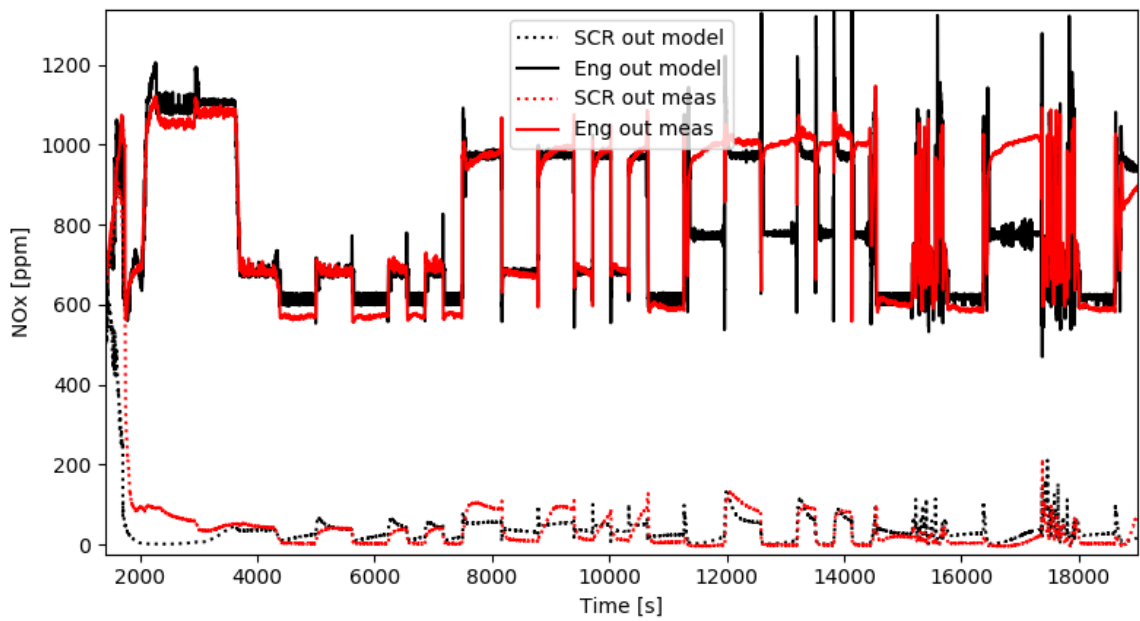


Figure 23: NOx exhaust (before SCR, solid) and tailpipe (after SCR, dashed) emissions: measurement (red) vs. virtual engine (black).

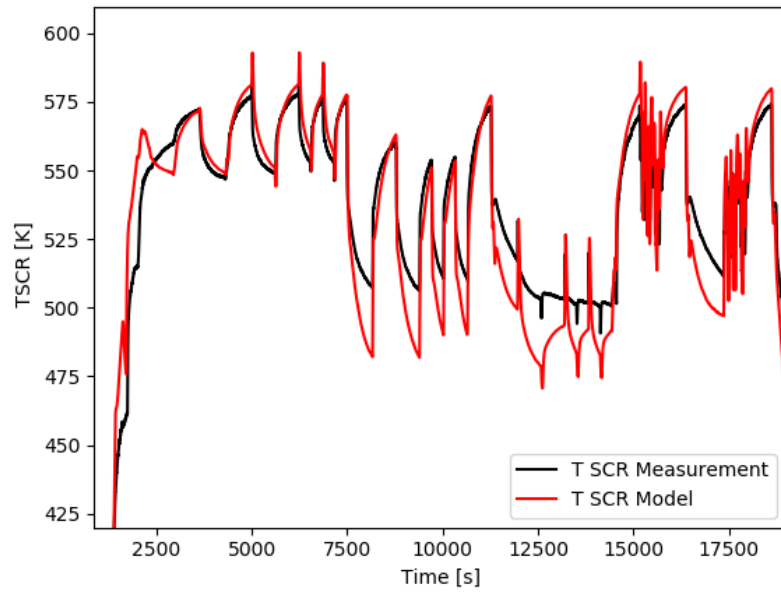


Figure 24: Comparison of modelled (red) and measured (black) SCR temperature.



4.3 Results dosing table & feed forward control

The present section presents the results from three different load cycles. In the first cycle (black color scheme), the SCR control is performed based on mapped emissions (Table 1, *DT*). In the second cycle (blue color scheme), the SCR is controlled with the NO_x freight calculated from the NO_x sensor and the measured exhaust mass flow with an alpha=0.9 (Table 1, *FF-0.9*), while in the third (purple colour scheme) the same control method is used with an alpha=0.95 (Table 1, *FF-0.95*). In the fourth cycle (green color scheme), the SCR is controlled using the NO_x freight from the PVS only (Table 1, *FF-PVS-0.9*).

Map based control (*DT*)

The dosing control for the SCR reaction is map based (*DT*) as shown in Figure 25. The NH₃ dosing amount is fixed depending on load, which means that each load condition assumes a pre-set value of NO_x to control the urea injection. This pre-set values of urea injection were determined using data from previous measurement campaigns. A linear interpolation provides the values between the measured conditions. This strategy is often used in applications where fuels are used which do not permit a direct measurement of the NO_x emissions or where emission regulations are lenient. The strategy requires a high repeatability of the NO_x-load-relationship.

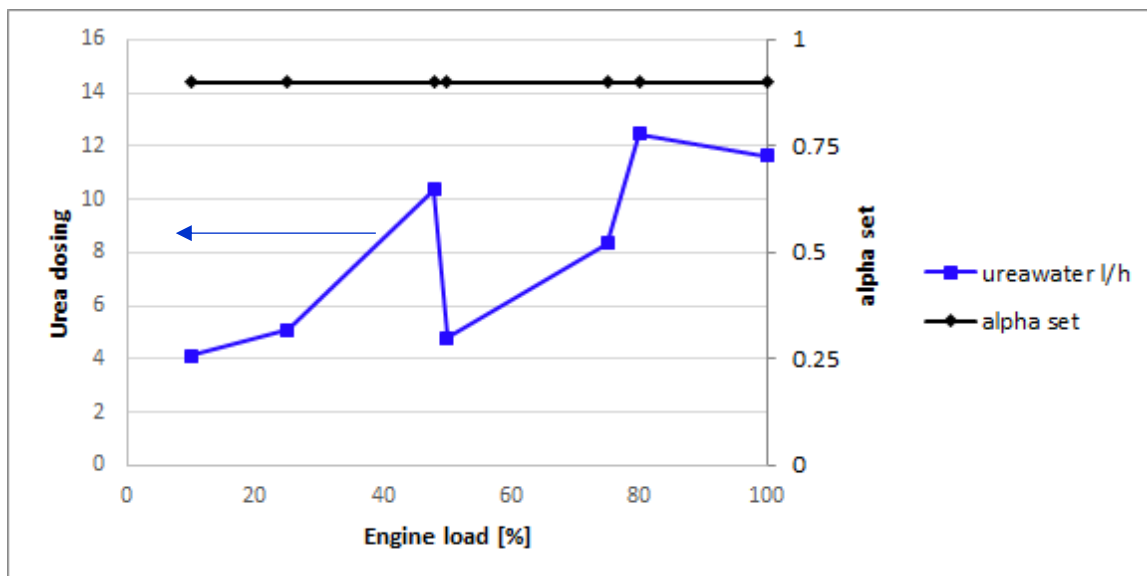


Figure 25: Dosing control strategy for the *DT* test: Urea dosing at various load points for an alpha set to 0.9.

Figure 26 shows the cycle load (top left), the exhaust- and tailpipe NO_x (top and bottom right respectively) with the *DT* control strategy. In order to be able to compare the conversion rate with the other cycles, the start-up phase of the engine has been neglected, since the initial conversion efficiency and in particular, the ammonia slip (Figure 26, bottom left) is strongly dependent on the initial loading of the catalyst, i.e. the amount of stored ammonia from the previous campaign. The ammonia slip is on an acceptable level with 6.5 ppm on average, with maximum peaks below 18 ppm. The dosing table was established in previous test runs (e.g. during commissioning) where an alpha of 0.9 was anticipated. However, the raw NO_x of the engine is dependent on the daily conditions such as humidity and temperature, as well as minor changes in engine performance over time due to component aging. A chosen alpha of 0.9 can therefore vary between approx. 0.88 - 0.99.

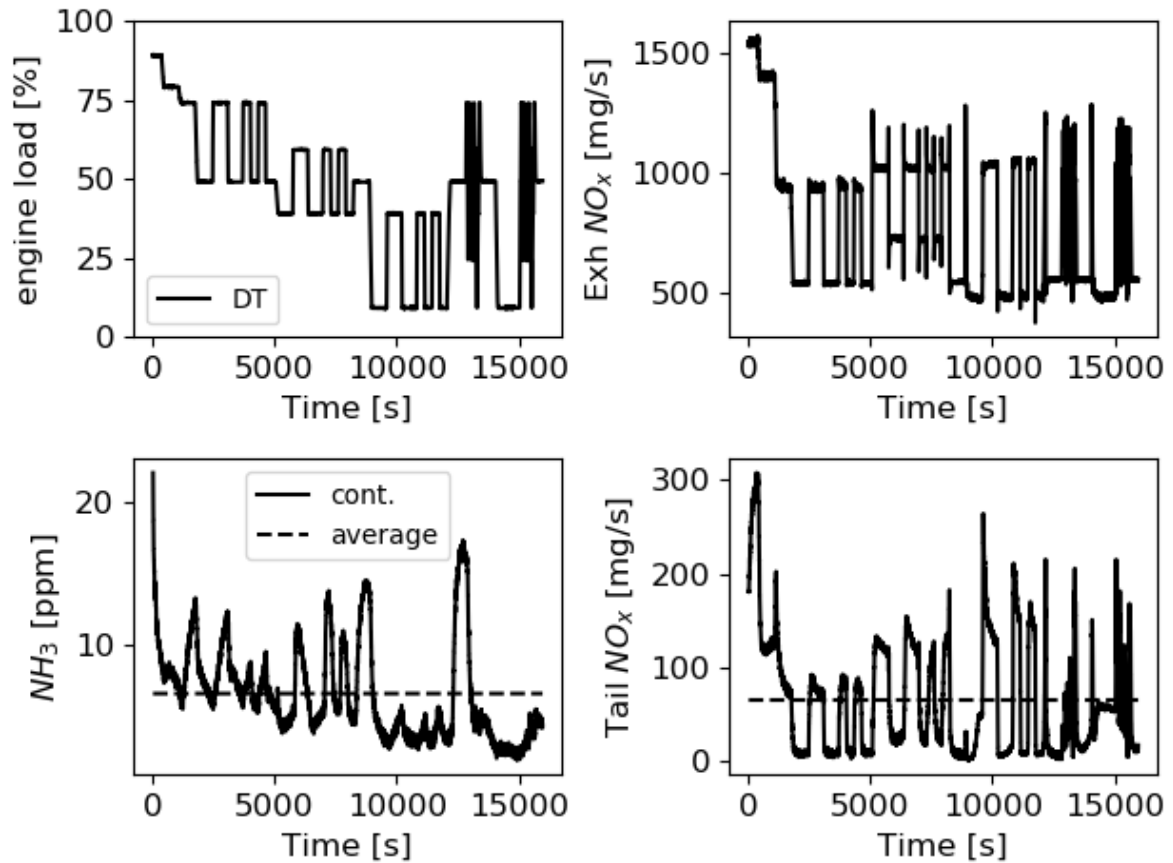


Figure 26: Dosing table cycle (*DT*); top left: engine load, top right: exhaust NO_x, bottom left: NH₃ slip (solid continuous, dashed average), bottom right tailpipe NO_x (solid continuous, dashed average). Entire cycle, starting from 90% load.

The main parameters of each load point are summarized in Figure 27. For each load point, the data was averaged. Due to the pre-set dosing table prior to the measurement campaign, a targeted alpha of 0.9 was not achieved and depending on the load point, the dosing varied between 0.93 and 0.99 with an average of approx. 0.95. This explains the relatively high NO_x conversion (approx. 92%) during this test cycle. It further demonstrates that the *DT* dosing principle is not sufficiently precise for systems with stringent regulations.

The NH₃ slip ranged from 2 to approx. 11 ppm, heavily depending on the load point. At 40% load, conversion and the alpha are deviating to a certain extent, which could generate a high NH₃ slip. However, the NH₃ slip at this load point was very low (approx. 4 ppm). The reason for this phenomenon is the very low temperature at this load point (approx. 240°C). Instead of NH₃ slip, the NH₃ was stored on the catalyst. This further explains the NH₃ slip peaks between 5000s and 10000s in Figure 26. Each load change from 40 to 60% increased the temperature by approx. 40°C, releasing a big part of the stored NH₃. As a consequence of the increased temperature and the NH₃ stored prior to the 60% load point, the NO_x conversion at 60% load was higher than the alpha dosed. Previously stored NH₃ could be used to convert the arriving NO_x at this load point.

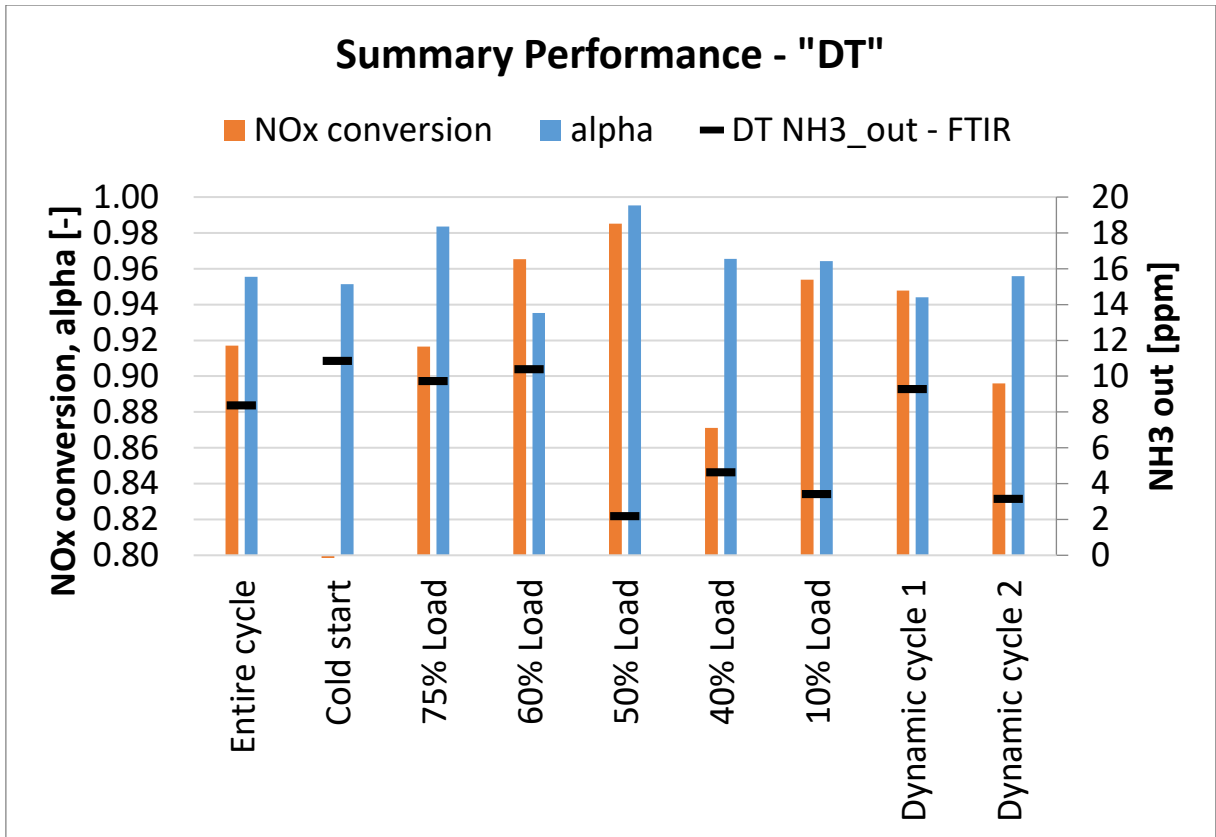


Figure 27: Average NO_x conversion, alpha and NH₃_out during the steady state part of the DT cycle as well as the dynamic part of the DT cycle.

4.3.2

Feed forward control (*FF=0.9*)

For the urea dosing of the FF control, a feedforward controller has been implemented by Hug Engineering. The NH₃ dosing is calculated from the corresponding NO_x freight (measured by a NO_x sensor and intake flow measurement on the engine) and a specific alpha can be set. Figure 28 shows the NO_x emissions (exhaust as well as tailpipe) over the entire cycle with an alpha set to 0.9. The figure additionally shows the corresponding ammonia slip (bottom left). As in the previous test, the average values are determined without considering the start-up phase. The peak ammonia slip is below 10 ppm. The NO_x reduction performance of the map-based approach would not have been expected to perform similarly, since the exhaust NO_x emission level has changed considerably.

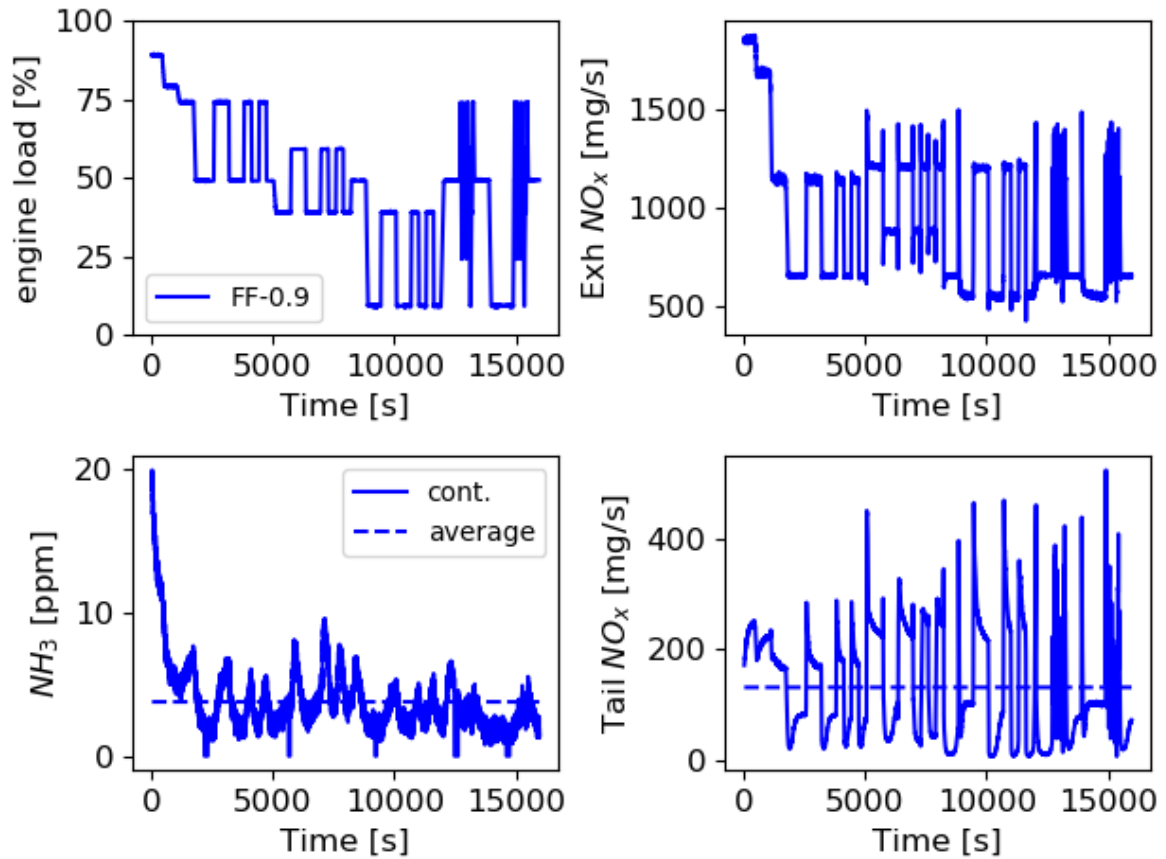


Figure 28: Feedforward cycle 0.9 (*FF-0.9*); top left: engine load, top right: exhaust NO_x, bottom left: NH₃ slip (solid continuous, dashed average), bottom right tailpipe NO_x (solid continuous, dashed average). Entire cycle, starting from 90% load.

The main parameters of each load point for the *FF-0.9* cycle are summarized in Figure 29. For each load point, the data was averaged. Due to the feedforward controller, the alpha remained unchanged over the entire cycle (approx. 0.88). Since the overall dosing is lower compared to the *DT* cycle in Figure 27, the NH₃ slip remains at a low level. The main difference between the load points were found in the NO_x conversion (Figure 29). Especially at 50 and 60% load, the conversion peaked with approx. 5% higher compared to the alpha. At these load points, the temperatures were higher compared to 75, 40 and 10% (Figure 40) and previously stored NH₃ can react with NO_x according to the SCR reaction. This excess of NH₃ results in a higher NO_x conversion efficiency than provided by the freshly dosed NH₃ at alpha 0.88.

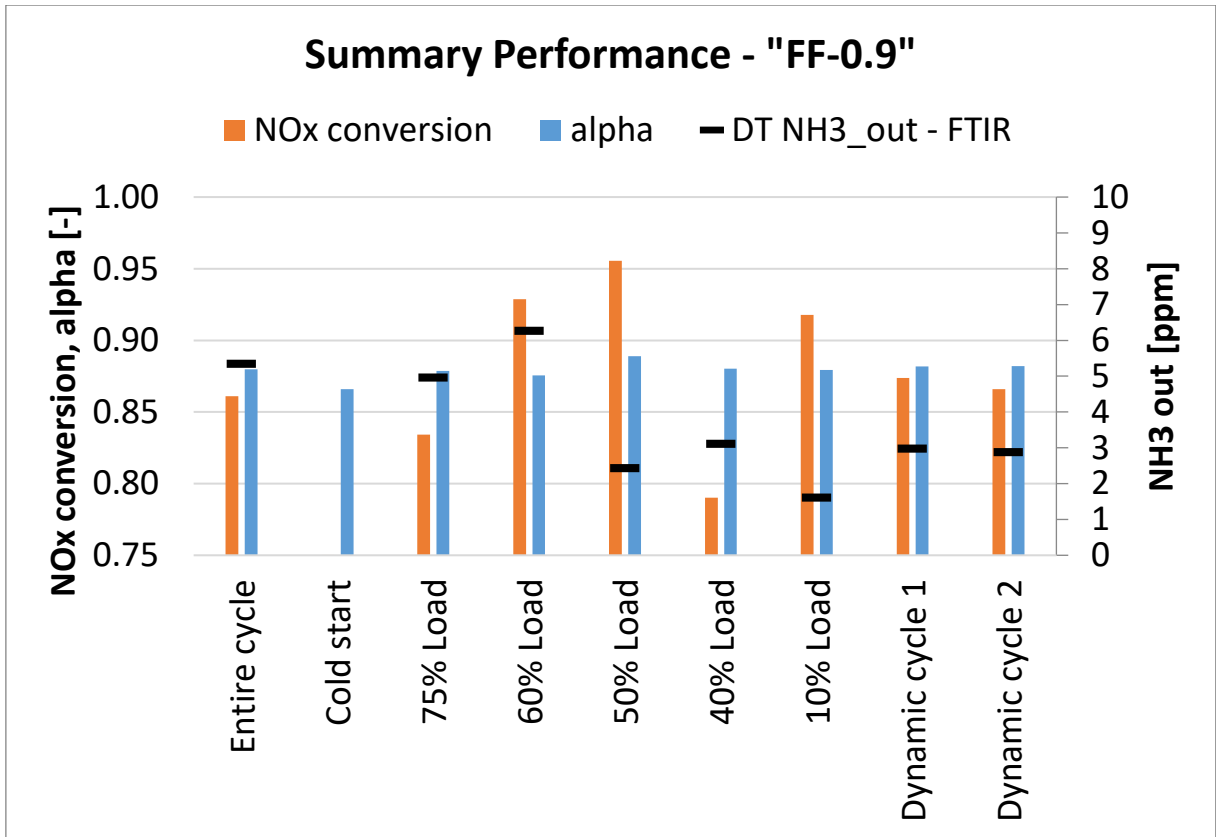


Figure 29: Average NO_x conversion, alpha and NH₃_out during the steady state part of the FF-0.9 cycle as well as the dynamic part of the FF-0.9 cycle.

4.3.3

Feed forward control (FF-0.95)

A second cycle with the feed forward control strategy has been recorded to better evaluate the catalyst's performance. Again Figure 30 displays the load, NH₃ slip (top and bottom left respectively) as well as the exhaust- and tailpipe NO_x emissions (top and bottom right respectively). In contrast to the FF-0.9 strategy, the FF-0.95 strategy is performed with a higher ammonia dosing level. This strategy was mainly applied to detect the catalyst's performance limit with an ammonia slip limit. The figure reveals lower NO_x tailpipe emissions and higher average as well as peak ammonia slip. This means, that a further increase in ammonia dosing would lead to excessive ammonia slip without further increase in NO_x reduction. This cycle shows the trade-off behaviour between NO_x reduction and NH₃ slip.

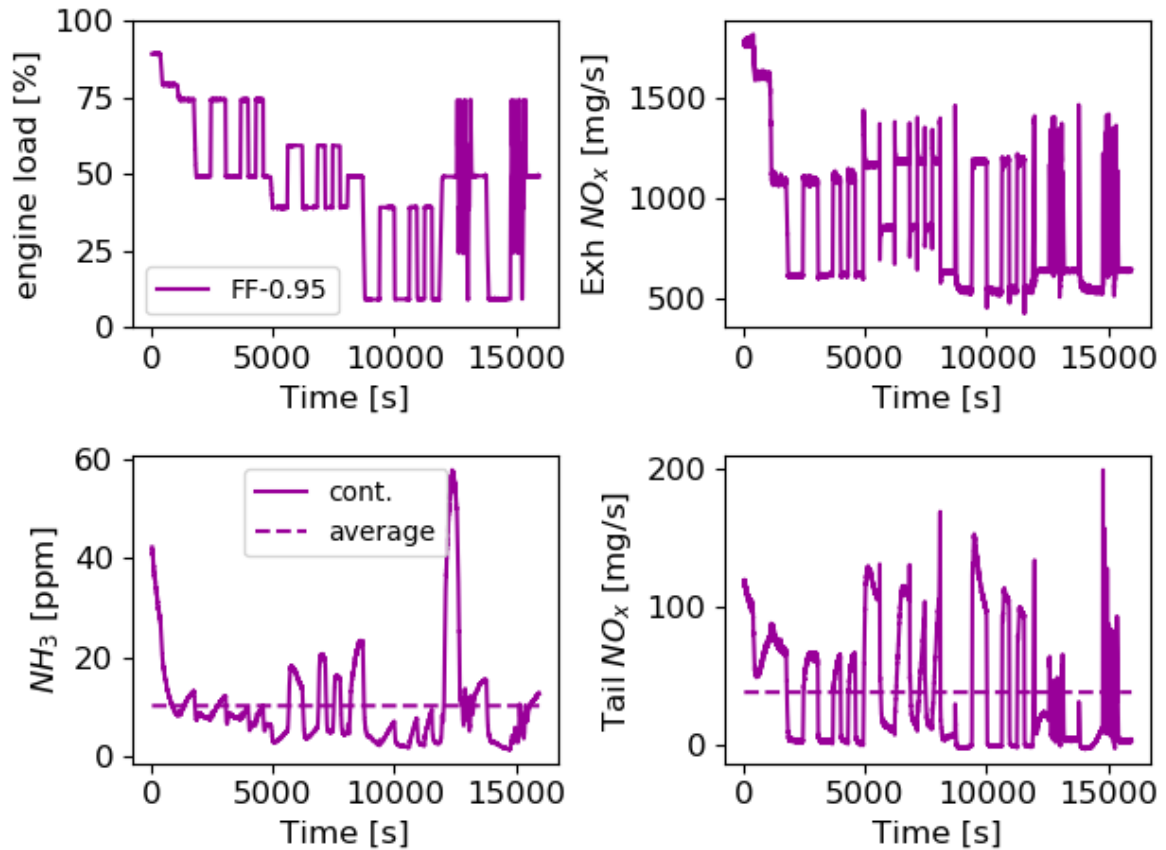


Figure 30: Feedforward cycle 0.95 (*FF-0.95*); top left: engine load, top right: exhaust NO_x, bottom left: NH₃ slip (solid continuous, dashed average), bottom right tailpipe NO_x (solid continuous, dashed average). Entire cycle, starting from 90% load.

The main parameters of each load point for the *FF-0.95* cycle are summarized in Figure 31. For each load point, the data was averaged. Due to the feedforward controller, the alpha remained at around 0.94 and was not influenced by external effects as seen with the *DT* principle in Figure 27. As already mentioned, compared to *FF-0.9* in Figure 29, the *FF-0.95* cycle was tested with a higher alpha, which resulted in higher NH₃ slip and higher NO_x conversions. Since the overall dosing is also higher compared to the *DT* cycle, the NH₃ slip increased to above 10 ppm on average. At many load points, the NO_x conversion was higher compared to the alpha dosed. This can be explained by the generally high alpha over the entire cycle and the low temperature. During the cold start, the entire catalyst was filled with NH₃ (the NO_x conversion remained very low), which could be used in later stages of the cycle to generate higher NO_x conversions. The load point at 40% is different to the other load points. A low NO_x conversion was measured which can be explained by the very low temperature of 240°C. At 10% load, the temperature was identical to the 40% load point but the NO_x conversion was above 99%. Since the total mass flow was heavily reduced a very low space velocity over the catalyst was generated. This is equivalent to a higher catalyst volume, hence more time for the catalyst to reduce the exhaust NO_x. To that end, the 10% load point generated much less NO_x (Figure 30), hence the alpha 0.95 together with the stored NH₃ was sufficient to reduce NO_x effectively.

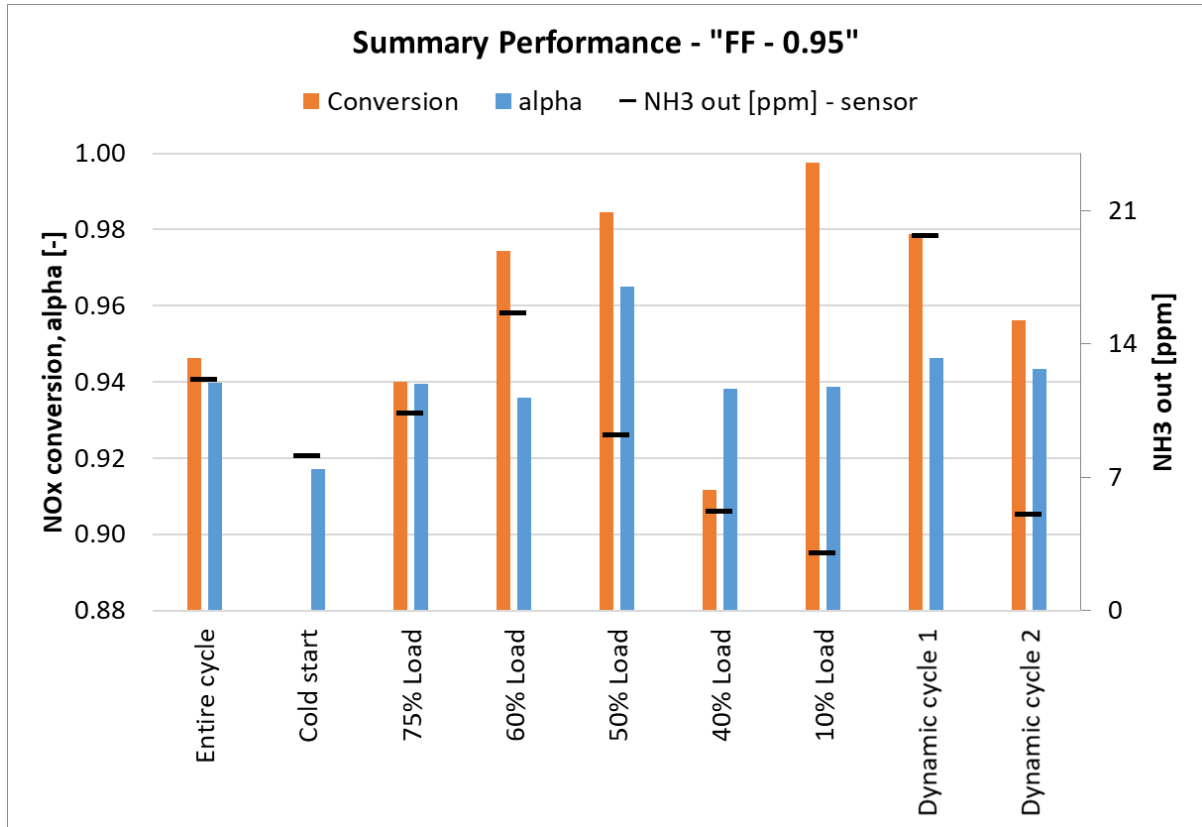


Figure 31: Average NO_x conversion, alpha and NH₃_out during the steady state part of the *FF-0.95* cycle as well as the dynamic part of the *FF-0.95* cycle

4.3.4

Feed forward control (*FF-PVS*)

Figure 32 shows the NO_x exhaust and tailpipe emissions (right top and bottom) and the corresponding ammonia slip (left bottom) with the *FF-PVS* dosing strategy. Identical to the *FF-sensor* strategy, the NH₃ dosing is calculated from the NO_x freight. In this strategy however, the NO_x freight is entirely calculated from the PVS, using modelled NO_x concentration and calculated exhaust flow rates. In comparison to the *FF* control strategy using a sensor, the conversion efficiency is slightly higher (91%) while the ammonia slip is 5 ppm on average. The minor change in conversion efficiency and ammonia slip are attributed to the positive offset between the *FF-PVS* and the *FF* measured NO_x freight. However, the PVS has proved to have the required signal quality, accuracy and stability to enable an SCR feedforward control with a reference abatement of 90%. Figure 32, top right shows the NO_x freight from measurements and from the PVS during the *FF-PVS* cycle. This time, only the PVS is used as input for the SCR control. This setup is in particular advantageous using heavy fuel oil and allows a feedforward-controlled SCR in installations where a conventional sensor would display a strongly restricted life time. The initial PVS parameters have already been calibrated from the previous cycle. In general, all these strategies suffer a high fluctuation of conversion efficiency and ammonia slip, since the catalyst reaction time is slower than the change in NO_x freight from the engine. This issue is addressed in the optimization procedure.

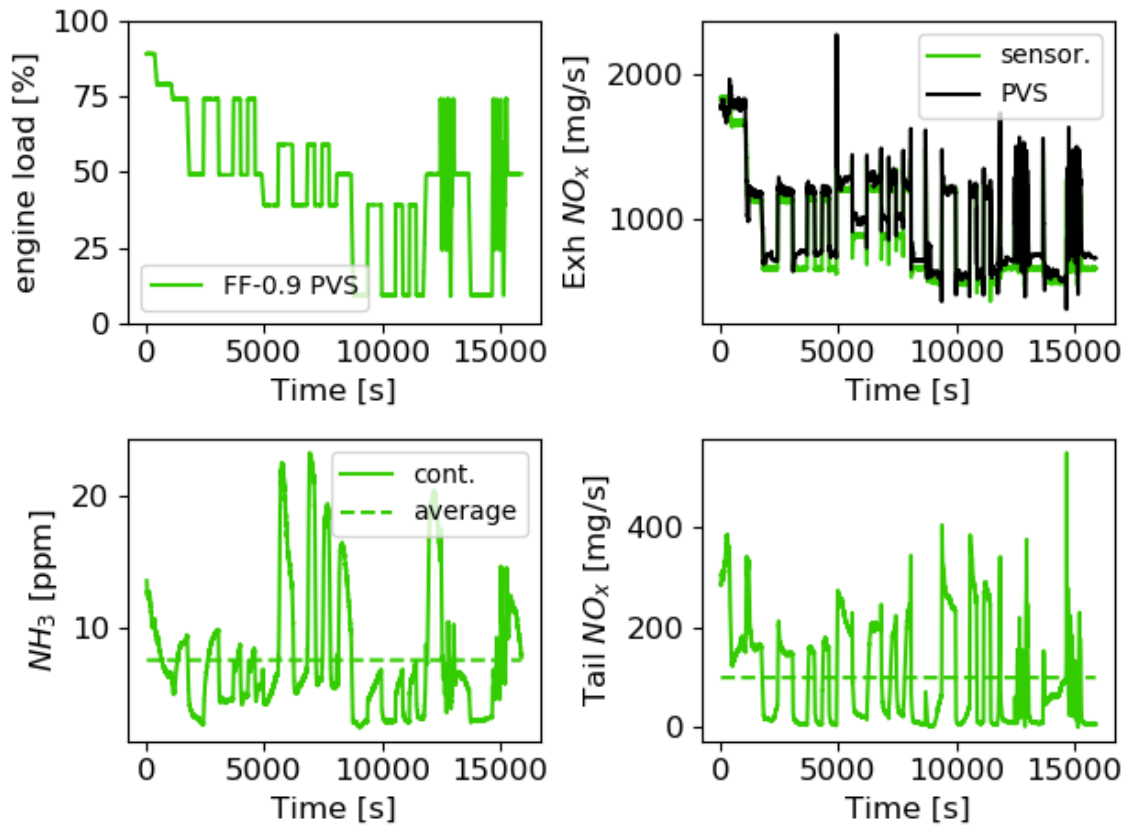


Figure 32: Feedforward cycle 0.9 with PVS as source of NO_x freight (*FF-0.9 PVS*); top left: engine load, top right: exhaust NO_x (black PVS, light green sensor), bottom left: NH₃ slip (solid continuous, dashed average), bottom right tailpipe NO_x (solid continuous, dashed average). Entire cycle, starting from 90% load.

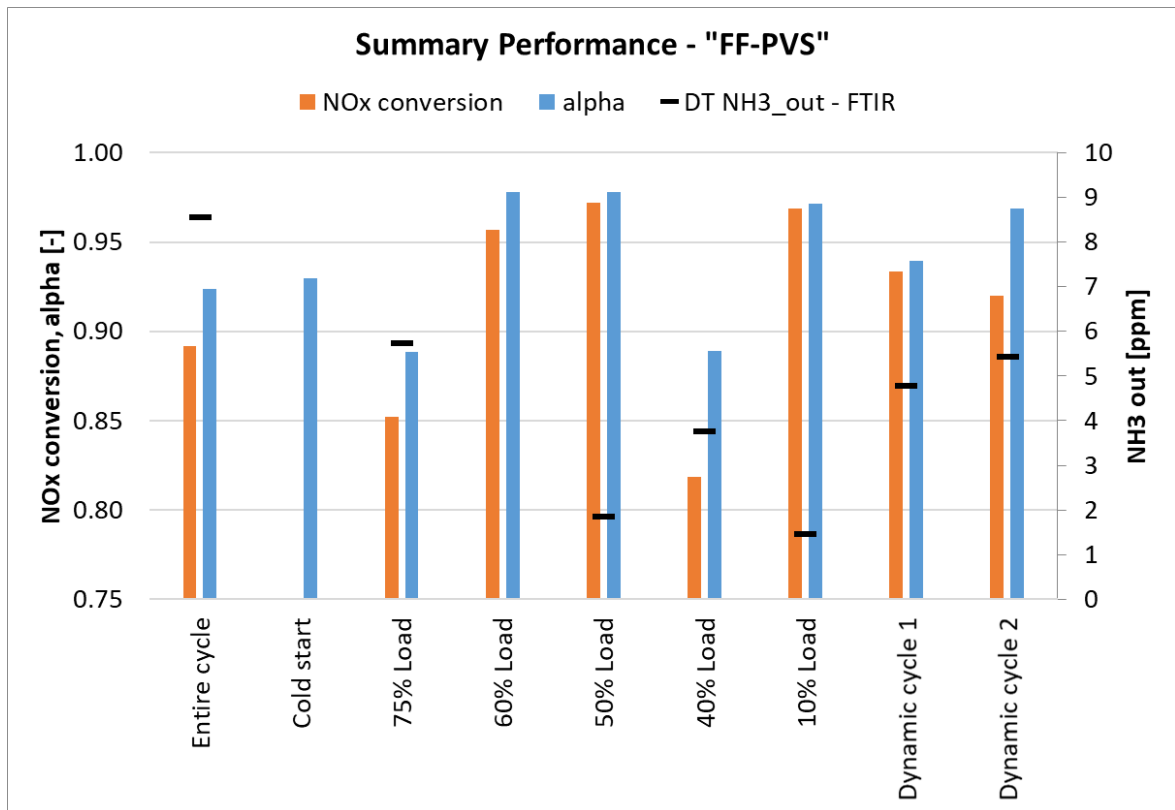


Figure 33: Average NO_x conversion, alpha and NH₃_out during the steady state part of the FF-0.95 cycle as well as the dynamic part of the FF-PVS cycle

4.4 Results after optimization

This section provides the results achieved using the optimized engine setup. The section is split in two sub-sections, providing the results of the offline optimization (*Off Opt*), the hybrid off/online optimization (*Hyb Opt*).

Offline optimization

Figure 34 shows engine load (top, left), the NO_x exhaust and tailpipe emissions (right, top and bottom) and the corresponding ammonia slip (left, bottom) with the offline optimized engine operation (Table 1, *Off Opt*). The cycle shows a very low tail pipe NO_x level and a rather high NH₃ level, with some extreme spikes. The reason for this lies partwise in the implementation and partwise in the concept of the strategy. The urea dosing has been established using the simulated possible conversion efficiency under the expected temperature and mass flow level. Therefore, the transient behaviour of the catalyst is neglected (conceptual issue). In addition, by omission, no margin from the calculated to the effective urea dosing was set (implementation issue). The NH₃ emissions would be much lower with some additional margin of the urea dosing, without a significant decrease in NO_x reduction.

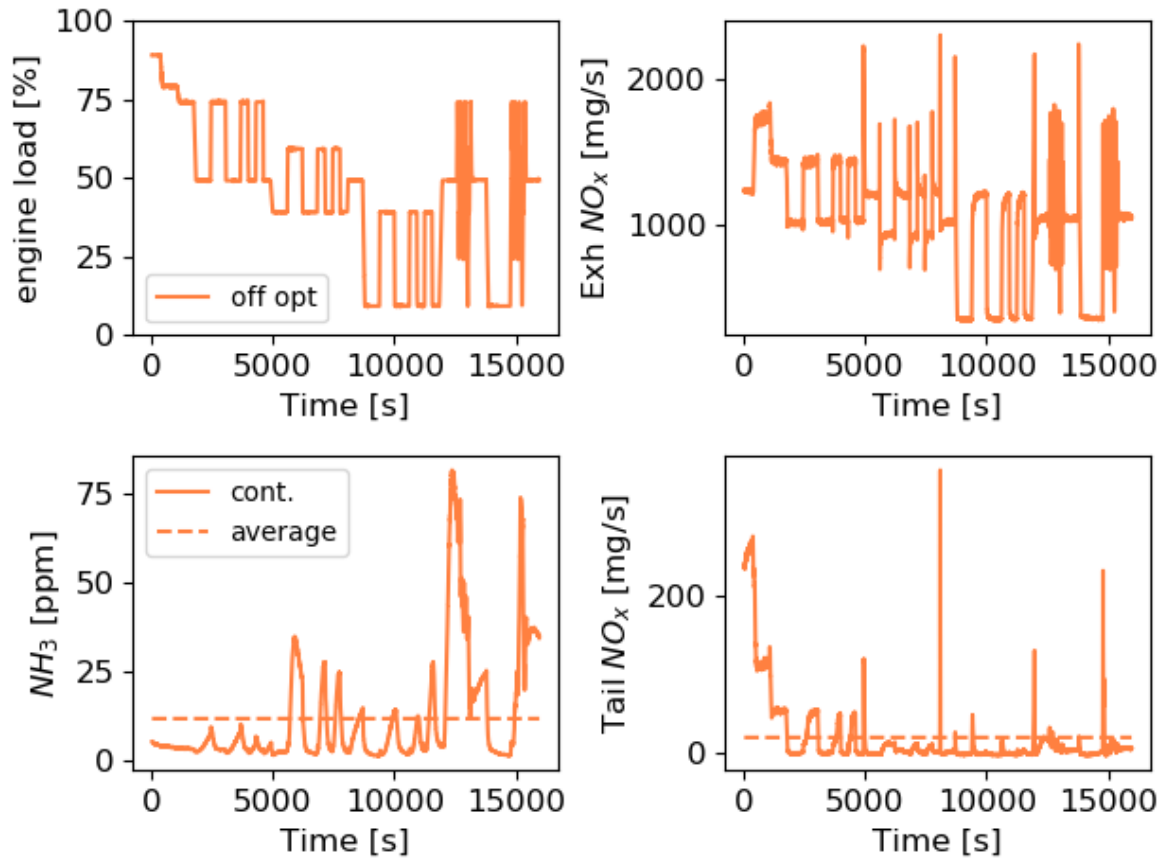


Figure 34: Offline optimized cycle (*Off Opt*, orange) in comparison to reference cycles (black: *DT* resp. purple *FF-0.95*); top left: engine load, top right: exhaust NO_x, bottom left: NH₃ slip (solid continuous, dashed average), bottom right tailpipe NO_x (solid continuous, dashed average). Entire cycle, starting from 90% load.

The main parameters of each load point for the “*Off Opt*” cycle are summarized in Figure 35. For each load point, the data was averaged. Due to the offline optimization and the feedforward controller, a high NO_x conversion for all load points could be achieved. The alpha was set equal to the maximum allowed NO_x conversion obtained from the SCR model during the offline optimization. (As an example: Max. NO_x conversion at 10 ppm NH₃ slip at given T = 98% → alpha = 0.98). The alpha measured was close to the NO_x conversion measured for most load points. Due to the high set point of alpha at most load points, the NH₃ slip was higher compared to *DT*, *FF-0.9* and also higher compared *FF-0.95*. On average, an alpha of almost 0.98 was set. The corresponding slip was approx. 14 ppm (incl. cold start) and the NO_x conversion was above 97%, on average. The data in Figure 35 clearly show that the offline optimization was successful and much better conversion rates could be achieved, especially at low loads. This could mainly be attained by changing the exhaust gas temperature at low load points using different WG settings (see Figure 49). The data further showed that the NH₃ dosing has to be adjusted in order to minimize the NH₃ slip.

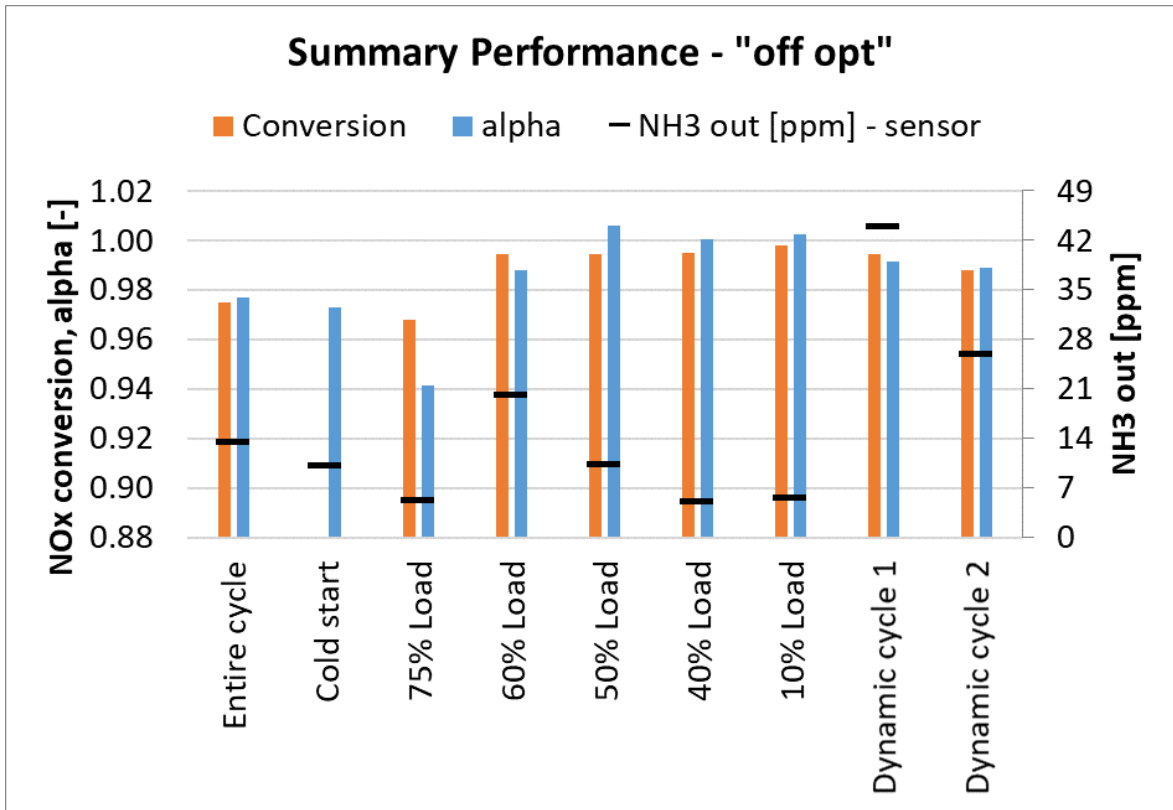


Figure 35: Average NO_x conversion, alpha and NH₃_out during the steady state part of the off-opt cycle as well as the dynamic part of the off-opt cycle

4.4.2

Hybrid off/online optimization *Hyb Opt*

Figure 36 shows engine load (top, left), the NO_x exhaust and tailpipe emissions (right, top and bottom) and the corresponding ammonia slip (left, bottom) with the offline optimized engine operation and online adapted catalyst (*Hyb Opt*). The figure also includes the PVS output since it was partly used as a source of NO_x freight for parts of the cycle. In contrast to the *Off Opt* strategy, the *Hyb Opt* strategy continuously adapts the urea dosing based on the catalyst's actual internal condition, which is determined with an online running SCR digital twin. This strategy shows low tailpipe NO_x emissions with simultaneous low ammonia slip. This is a significant improvement in NO_x reduction and ammonia slip trade-off behaviour. Approximately the first 4000 seconds and the first fast transient section (around 13000 seconds) are controlled using the PVS as source of NO_x freight, the rest was operated using the exhaust NO_x sensor. In this implementation the PVS software was recently updated and only partially calibrated.

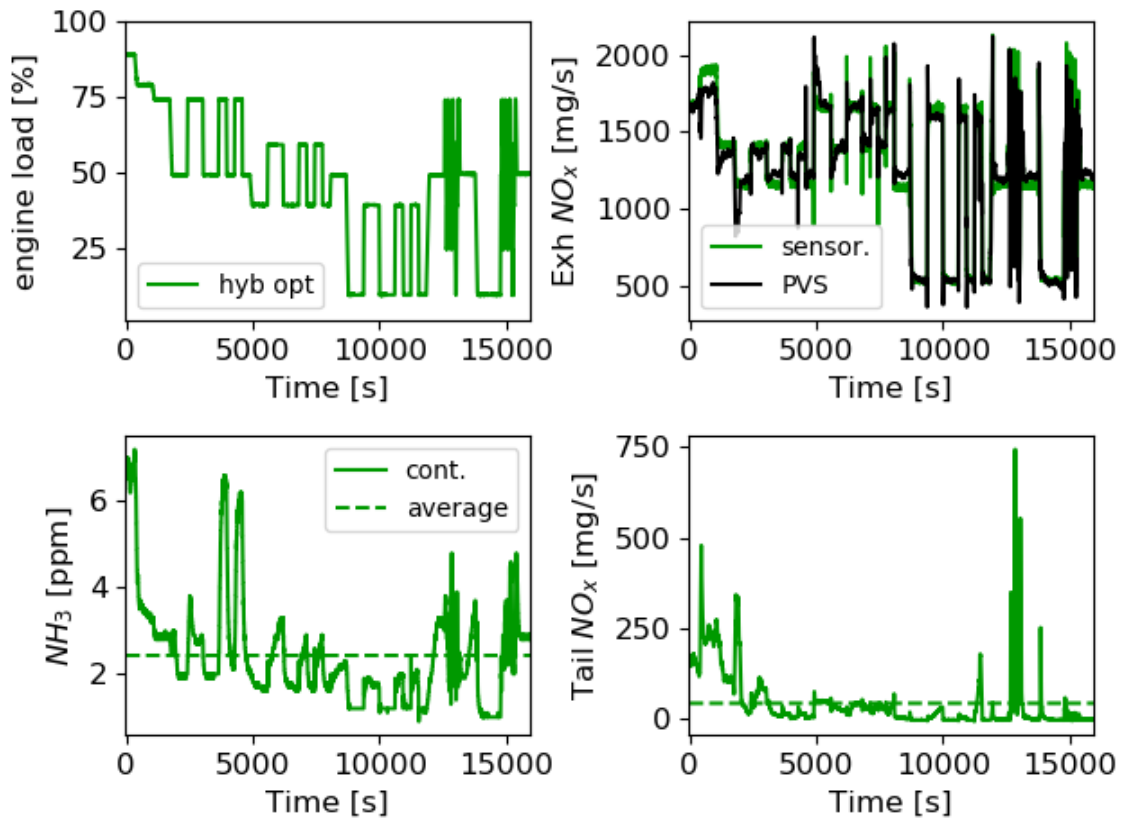


Figure 36: Hybrid optimized cycle (*Hyb Opt*); top left: engine load, top right: exhaust NO_x (black PVS, dark green sensor), bottom left: NH₃ slip (solid continuous, dashed average), bottom right tailpipe NO_x (solid continuous, dashed average). Entire cycle, starting from 90% load.

The impact of the PVS calibration is visible in Figure 37, showing a zoom of Figure 36 between 1000 and 2500 seconds. In this part of the cycle the load has just changed to 75%, followed by a change to 50%. In both loads, the PVS is adapting the internal model parameters to provide the NO_x freight accurately. The underestimation of the NO_x emissions at the beginning of the 50% load leads to a spike in tail pipe NO_x emissions.

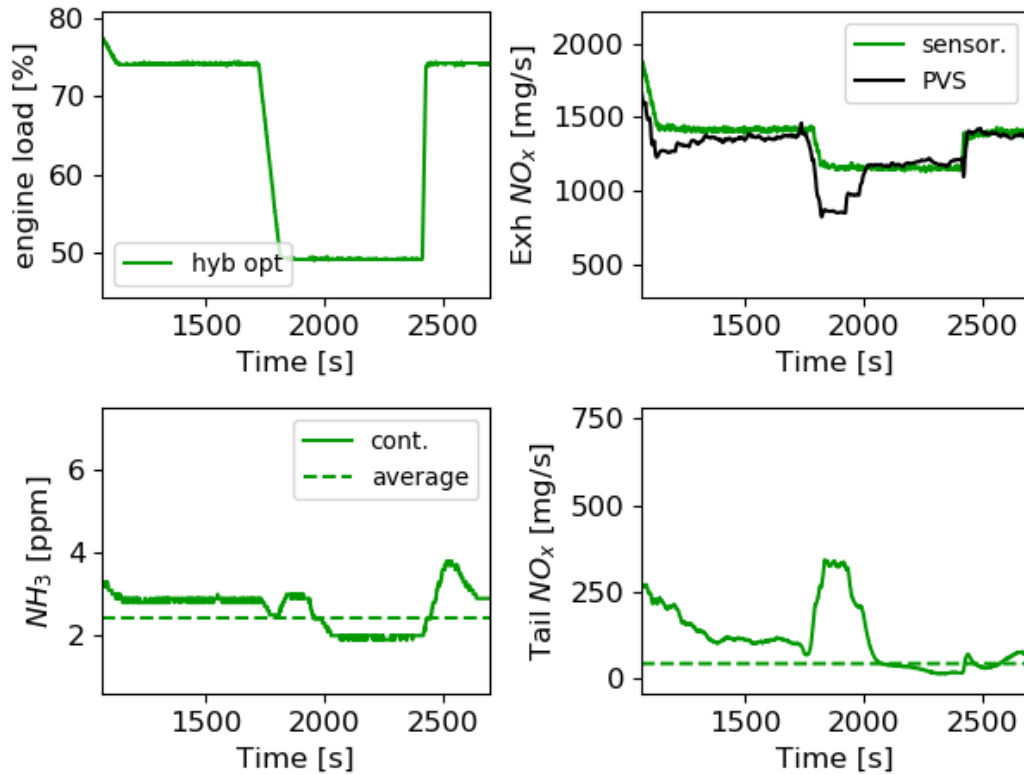


Figure 37: Hybrid optimized cycle (*Hyb Opt*); top left: engine load, top right: exhaust NO_x (black PVS, dark green sensor), bottom left: NH₃ slip (solid continuous, dashed average), bottom right tailpipe NO_x (solid continuous, dashed average). Zoom to first time 75% and 50%.

The impact of the PVS accuracy is also visible in Figure 38, showing a zoom of Figure 36 between 12400 and 13000 seconds. In this part of the cycle is the first fast transient section. The top right part shows the NO_x freight from the sensor versus the NO_x freight from the PVS. In general, the accuracy of the PVS is very good, only the 25% load point, which is not part of the rest of the cycle, is underestimated. This has a high impact on the tailpipe NO_x emissions and is visible in a spike.

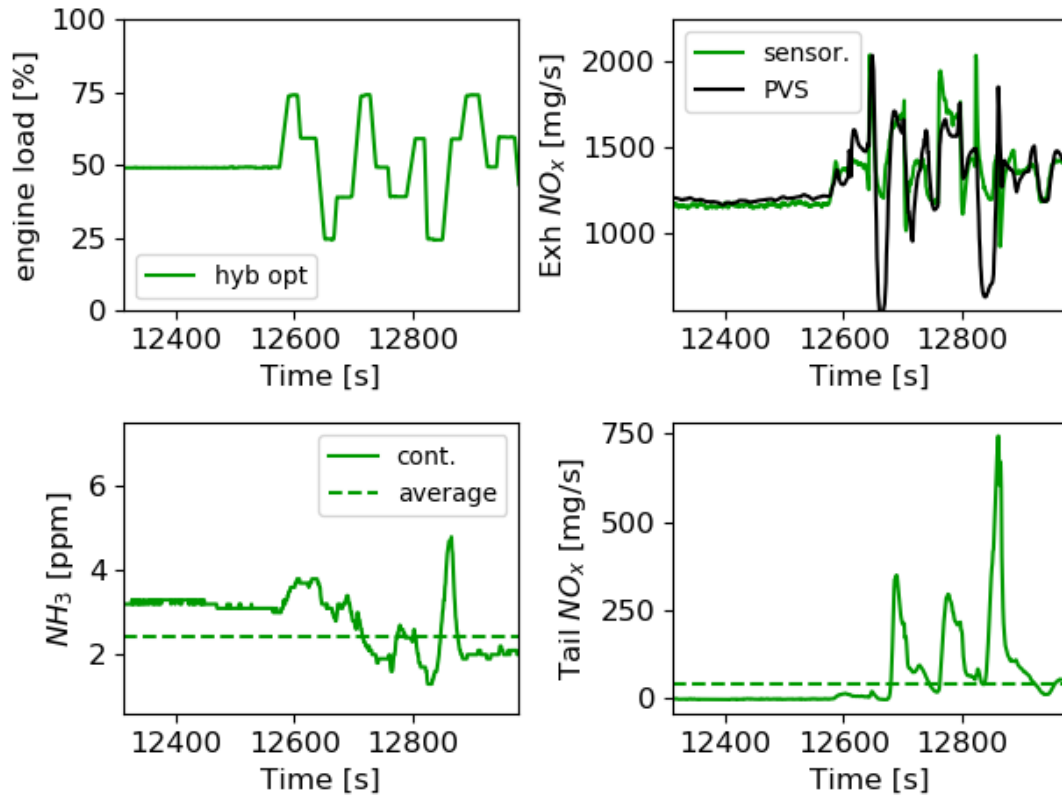


Figure 38: Hybrid optimized cycle (*Hyb Opt*); top left: engine load, top right: exhaust NO_x (black PVS, dark green sensor), bottom left: NH₃ slip (solid continuous, dashed average), bottom right tailpipe NO_x (solid continuous, dashed average). Zoom to first fast transient.

The two transients are compared in Figure 39, showing a zoom of Figure 36 between 12400 and 16000 seconds. The second transient uses the NO_x sensor as source for the NO_x freight determination. The tailpipe NO_x emissions during the entire transient are very low without significant rise of NH₃ emissions.

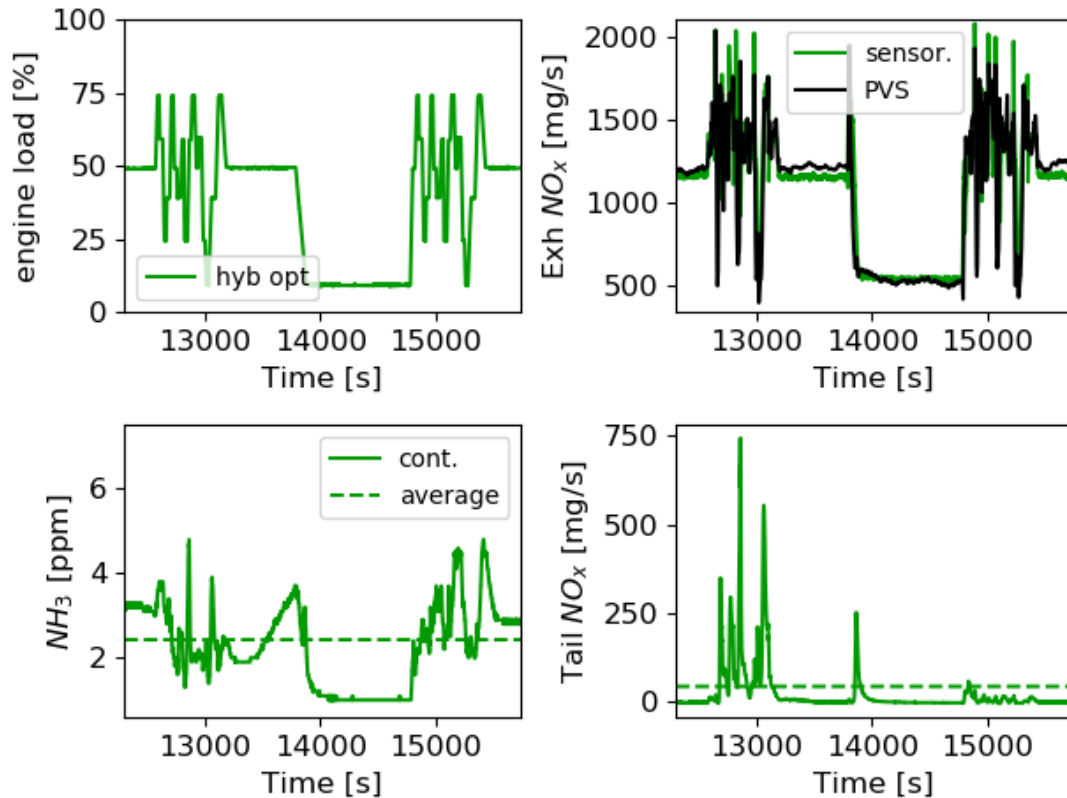


Figure 39: Hybrid optimized cycle (*Hyb Opt*); top left: engine load, top right: exhaust NO_x (black PVS, dark green sensor), bottom left: NH₃ slip (solid continuous, dashed average), bottom right tailpipe NO_x (solid continuous, dashed average). Zoom to compare the two fast transients.

The main parameters of each load point for the “*Hyb Opt*” cycle are summarized in Figure 40. For each load point, the data was averaged. Due to the offline & online optimization as well as the feedforward controller, a high NO_x conversion for all load points could be achieved. The alpha was set 2% lower to the maximum allowed NO_x conversion obtained from the SCR model during the offline optimization. (As an example: Max. NO_x conversion at 10 ppm NH₃ slip at given T = 98% → alpha = 0.96). The alpha measured was close to the NO_x conversion measured for most load points. Due to the reduced set point of alpha compared to the *Off Opt* cycle in Figure 35, the NH₃ remained at a very low level during the entire cycle (see also Figure 36). On average, an alpha of almost 0.97 was set. The corresponding slip was approx. 3 ppm (incl. cold start) and the NO_x conversion was above 94%, on average. The data in Figure 40 clearly show that the hybrid optimization was successful and much better conversion rates especially at low loads could be generated. This could mainly be achieved by changing the exhaust gas temperature at low load points (see Figure 49). The data further shows that the NH₃ dosing could be optimized compared to the offline optimization (Figure 35) which minimized the NH₃ slip.

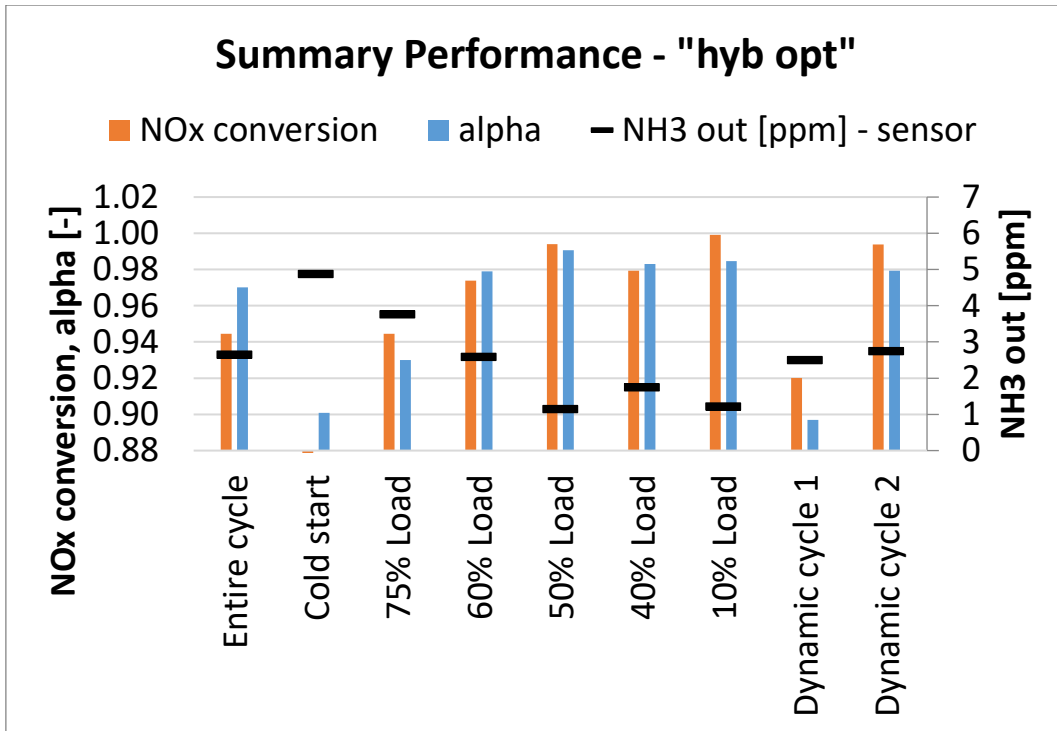


Figure 40: Average NO_x conversion, alpha and NH₃_out during the steady state part of the "Hyb Opt" cycle as well as the dynamic part of the Hyb Opt cycle.



4.5 Cycle comparison:

This section provides a comparison of the different strategies run during this project, focusing on performance in terms of NO_x reduction, NH_3 slip and fuel consumption.

Figure 41 shows a comparison between the reference cycle *DT*, the *FF-0.95* to show impact on NH_3 and NO_x spikes due to transient catalyst under and overload, and the *Off Opt* cycle. The *Off Opt* cycle shows higher NH_3 emissions as time in the cycle advances. The average is only minorly above the *FF-0.95*. The *Off Opt* shows very low tail pipe NO_x emissions and generally higher exhaust NO_x emissions. The spikes in NH_3 from the *Off Opt* cycle occur mostly at the same positions as in the *DT* and particularly in the *FF-0.95*.

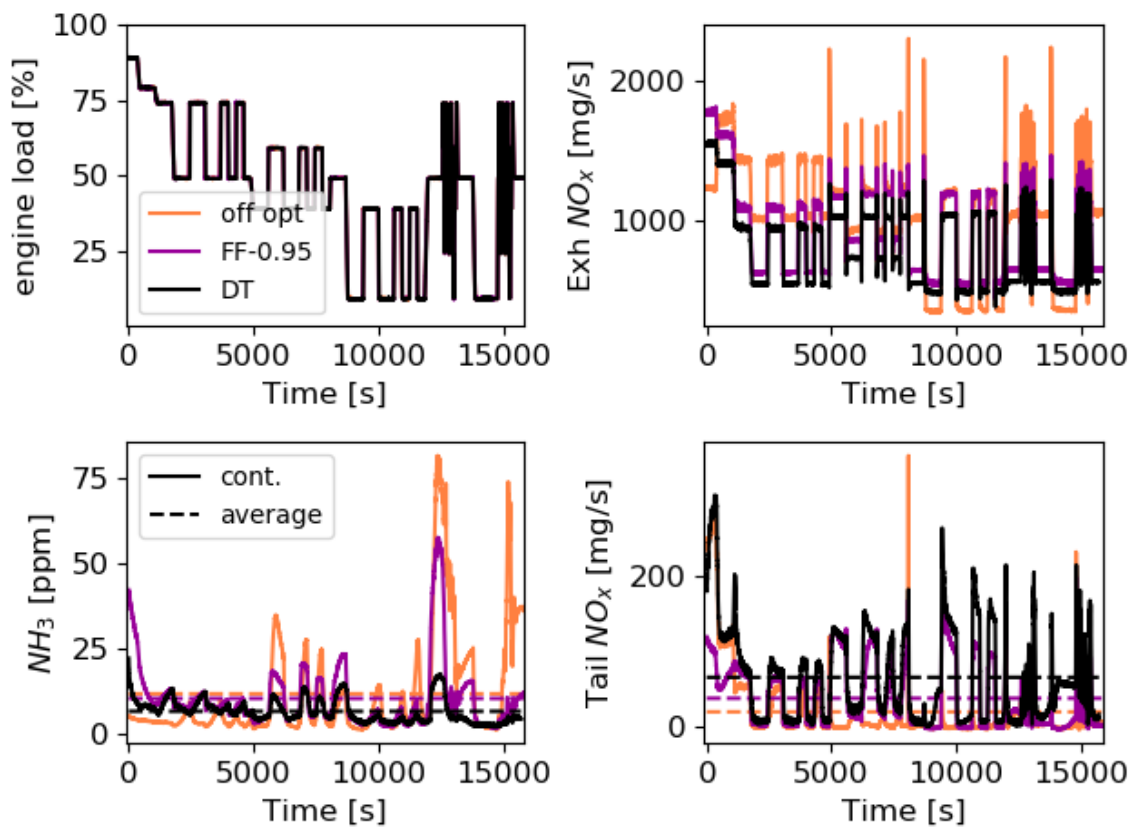


Figure 41: Offline optimized cycle (*Off Opt*, orange) in comparison to reference cycles (black: *DT* resp. purple *FF-0.95*); top left: engine load, top right: exhaust NO_x , bottom left: NH_3 slip (solid continuous, dashed average), bottom right tailpipe NO_x (solid continuous, dashed average). Entire cycle, starting from 90% load.



Figure 42 shows a zoom of Figure 41 into the second fast transient section of the cycle. NO_x exhaust emissions are higher in the case of the *Off Opt* cycle, except at 10% load operation. The tailpipe NO_x is extremely low after an initial spike. The NH_3 emissions show a very high peak in contrast to the reference cycles.

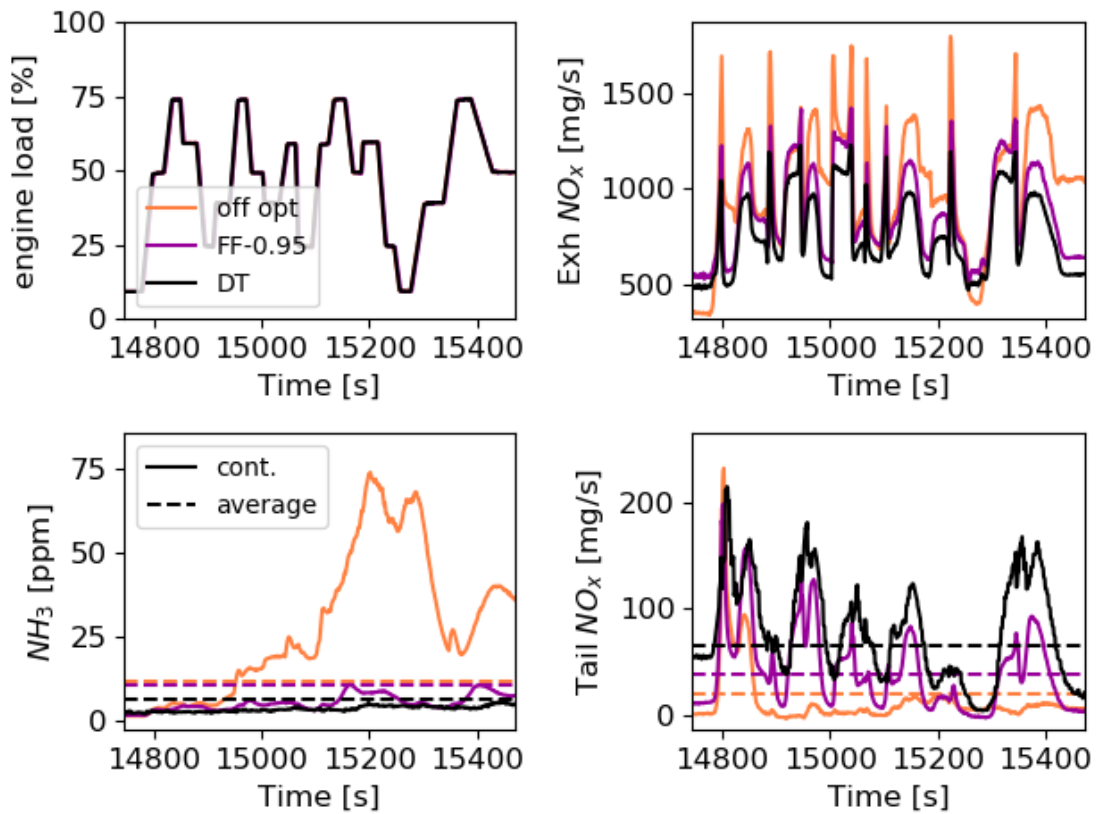


Figure 42: Offline optimized cycle (*Off Opt*, orange) in comparison to reference cycles (black: *DT* resp. purple *FF-0.95*); top left: engine load, top right: exhaust NO_x , bottom left: NH_3 slip (solid continuous, dashed average), bottom right tailpipe NO_x (solid continuous, dashed average). Zoom: second fast transient section



Figure 43 shows a comparison between the reference cycle *DT*, the *FF-0.95* and the *Hyb Opt* cycle. The *Hyb Opt* cycle shows very low NH_3 emissions without higher NO_x emissions in comparison to the other cycles (except during the previously discussed PVS calibration phase and the 25% load during the first fast transient section). Similar with the *Off Opt* cycle, the *Hyb Opt* cycle also shows significantly higher exhaust NO_x emissions in comparison to the reference cycles, which are reduced in the catalyst.

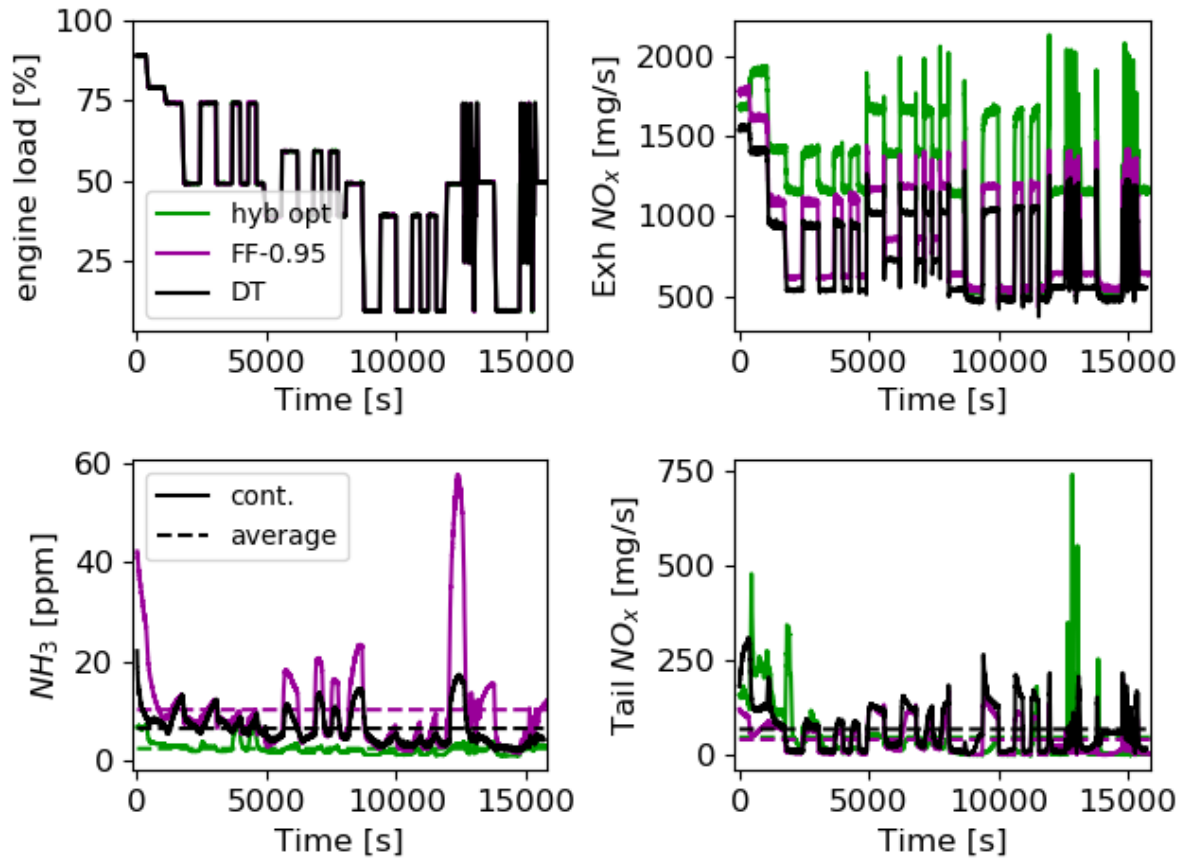


Figure 43: *Hyb Opt*, *FF-0.95* and *FF-0.9*; top left: engine load, top right: exhaust NO_x (green PVS, black sensor), bottom left: NH_3 slip (solid continuous, dashed average), bottom right tailpipe NO_x (solid continuous, dashed average). Entire cycle



Figure 44 shows a zoom of Figure 43 into the second fast transient section of the cycle. NO_x exhaust emissions are again higher in case of the *Hyb Opt* cycle except at 10% load operation. The tailpipe NO_x is extremely low without a significant initial spike. Simultaneously, the NH_3 emissions show similar or lower values compared to the reference cycles. This positive effect is attributed to the combination of the higher catalyst temperature (from the engine operating strategy) and the advanced urea dosing using the SCR digital twin.

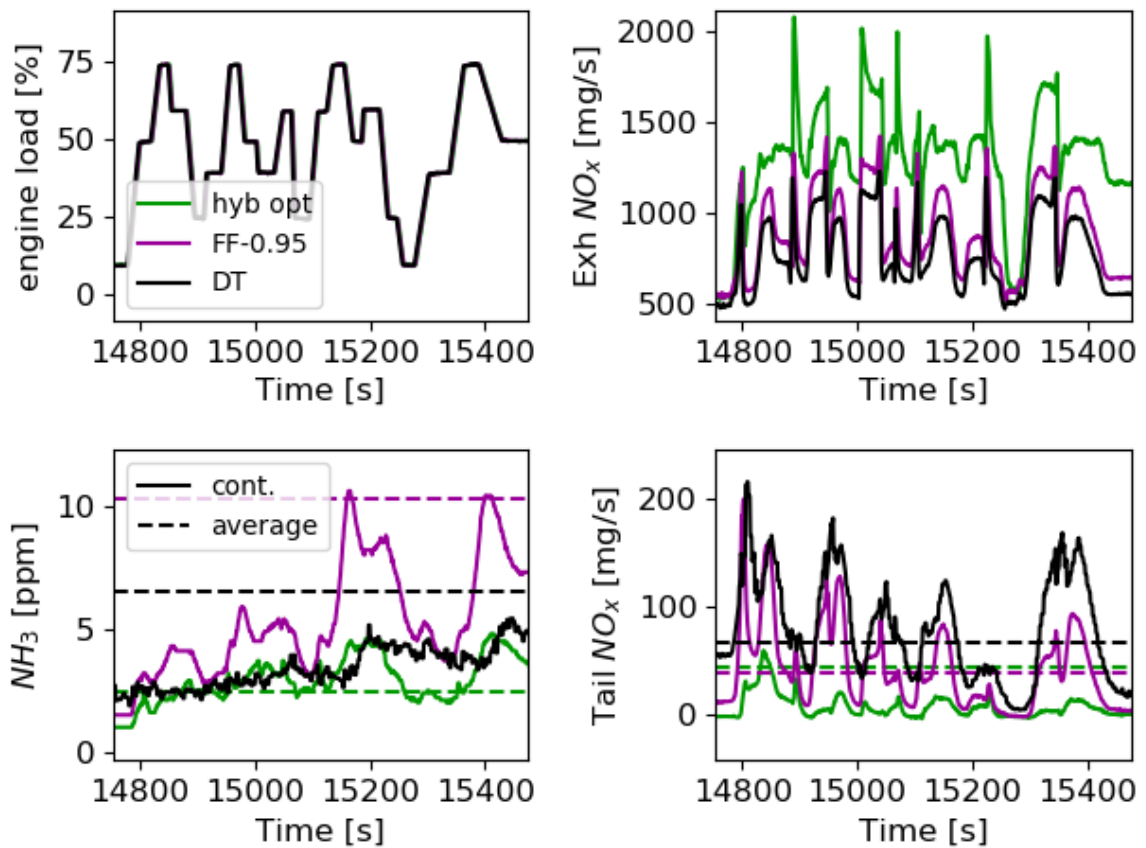


Figure 44: *Hyb Opt*, *FF-0.95* and *DT*; top left: engine load, top right: exhaust NO_x , bottom left: NH_3 slip (solid continuous, dashed average), bottom right tailpipe NO_x (solid continuous, dashed average). Zoom: second fast transient section.



Figure 45 shows the fuel consumption for the steady state points at the beginning of the cycle and the average through the entire cycle (without the cold start). The fuel consumption at 10% load is higher for both optimized strategies. The reason for this is the required exhaust temperature to achieve the required steady state temperature. In the cycle the 10% point is always after a higher load and therefore, the catalyst temperature is always hotter than expected in steady state. Therefore, the “investment” in high exhaust temperature from the optimization is exaggerated. The 50% and 60% point show a particular lower fuel consumption of the *Hyb Opt* in comparison to the references. The 60% and 90% point are particularly bad in the *Off Opt*. After this run, the model of the turbocharger has been recalibrated. The fuel consumption is generally more sensitive on WG position with increasing load. The overall benefit in fuel consumption from the *Hyb Opt* cycle in comparison with the *DT* is 0.8% (and 0.3% to the *FF-0.95*). The average fuel consumption of the total cycle is written in the plot in the corresponding colour.

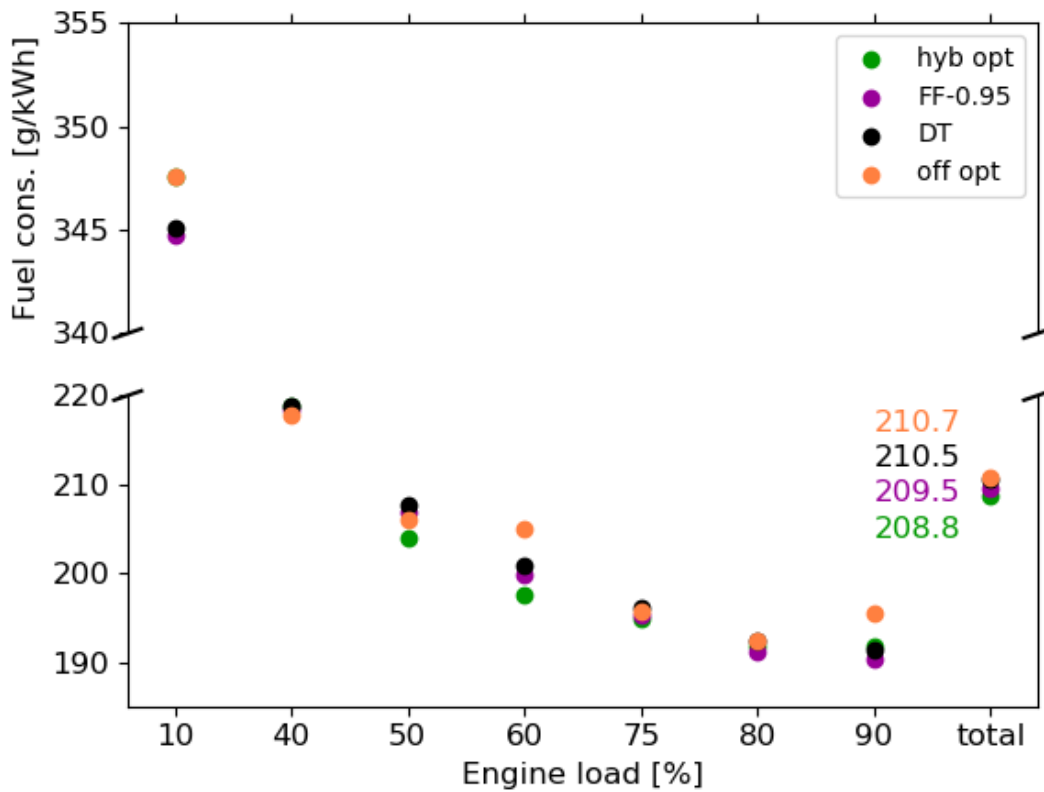


Figure 45: Fuel consumption of the steady state load points and the average over the entire cycle



Figure 46 shows the tailpipe NO_x emissions in g/kWh in a similar manner. The *Off Opt* strategy shows in the majority of the cases the lowest tailpipe NO_x emissions (in particular in the lower loads). The average tailpipe NO_x emissions of the *Off Opt* strategy is only 30% of the reference. Also the *Hyb Opt* cycle shows an average tailpipe NO_x emission reduction of roughly 50%. This is a similar reduction as from the *DT* strategy to the *FF-0.95*. The values of the total cycle are written in the figure in the corresponding colour.

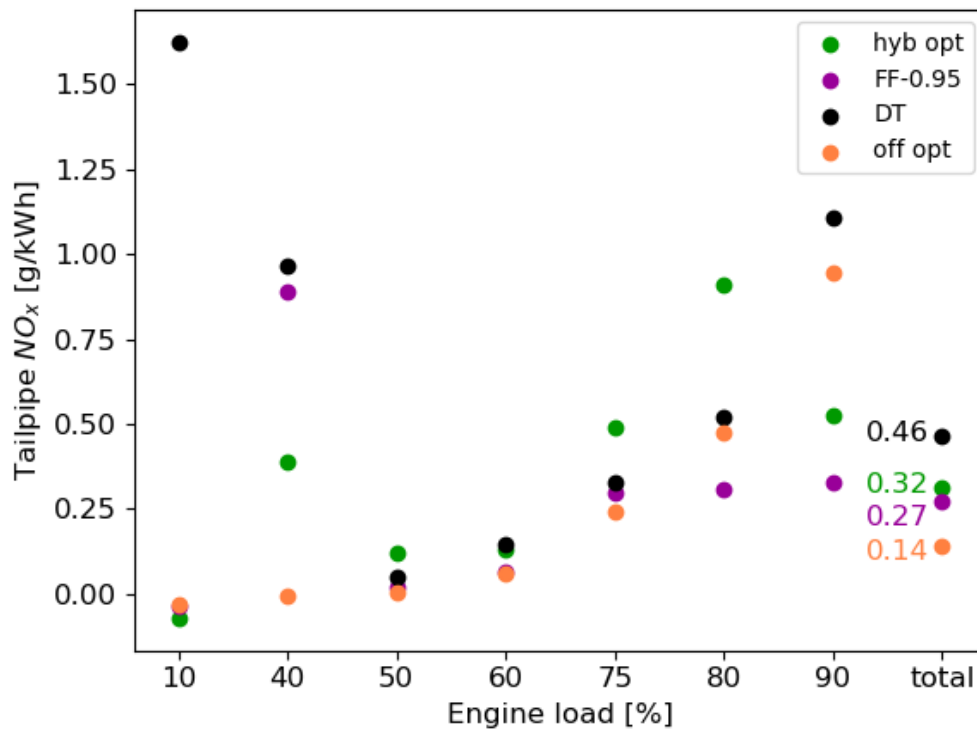


Figure 46: Tailpipe NO_x emissions of the steady state load points and the average over the entire cycle



Figure 47 shows the tailpipe NH₃ emissions in ppm. The *FF-0.95* strategy shows higher NH₃ slip in higher loads. The *Off Opt* strategy is particularly high at 60% under steady state conditions. The *Hyb Opt* strategy is the only one, which is below 10ppm in all points. Overall, the *Off Opt* and the *FF-0.95* show values minorly above 10ppm. The *Hyb Opt* strategy shows very low NH₃ slip during the entire cycle.

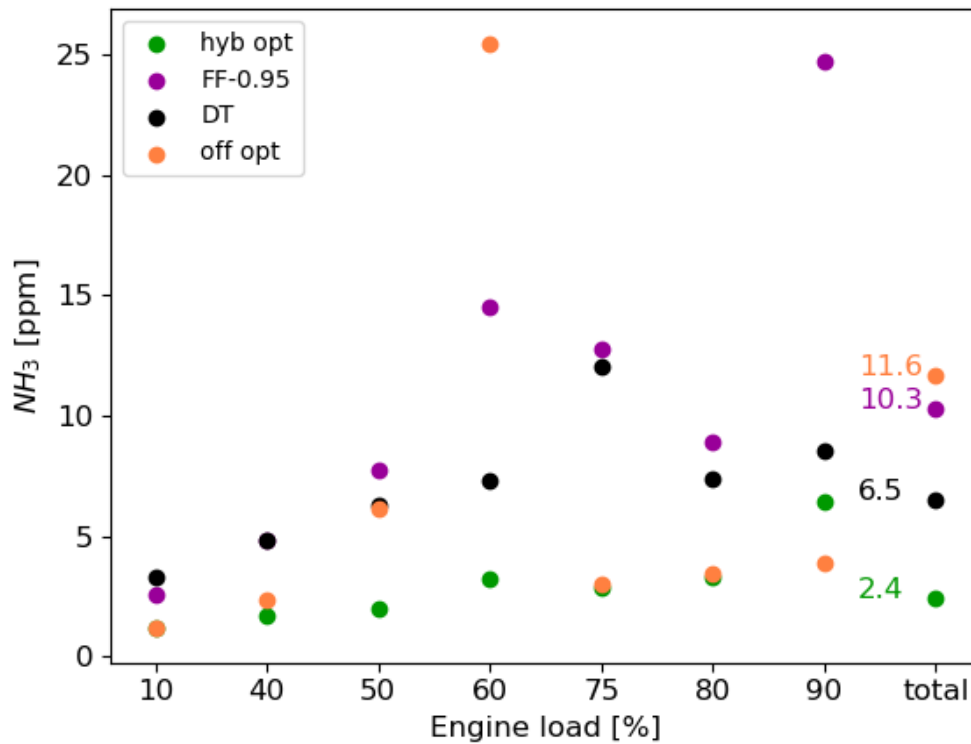


Figure 47: NH₃ concentration of the steady state load points and the average over the entire cycle



Figure 48 shows the engine-out exhaust NO_x emissions in g/kWh. The figure shows in general higher exhaust emissions from the optimized cycles, which is the consequence of the generally earlier injection timing. The earlier injection timing is required to balance or even improve the fuel consumption, since the wider open waste gate rather increase the fuel consumption. The wider open waste gate is required to increase the SCR temperature to allow higher NO_x conversion efficiency. This allows a reduced overall fuel consumption with a simultaneous reduction in tailpipe emissions and reduced ammonia slip. This is a very nice achievement, since these three quantities are typically in a trade-off. However, the price for this achievement are the exhaust NO_x. The overall exhaust NO_x emissions of the *Hyb Opt* cycle are increased by 20-25%. This also results in higher urea consumption.

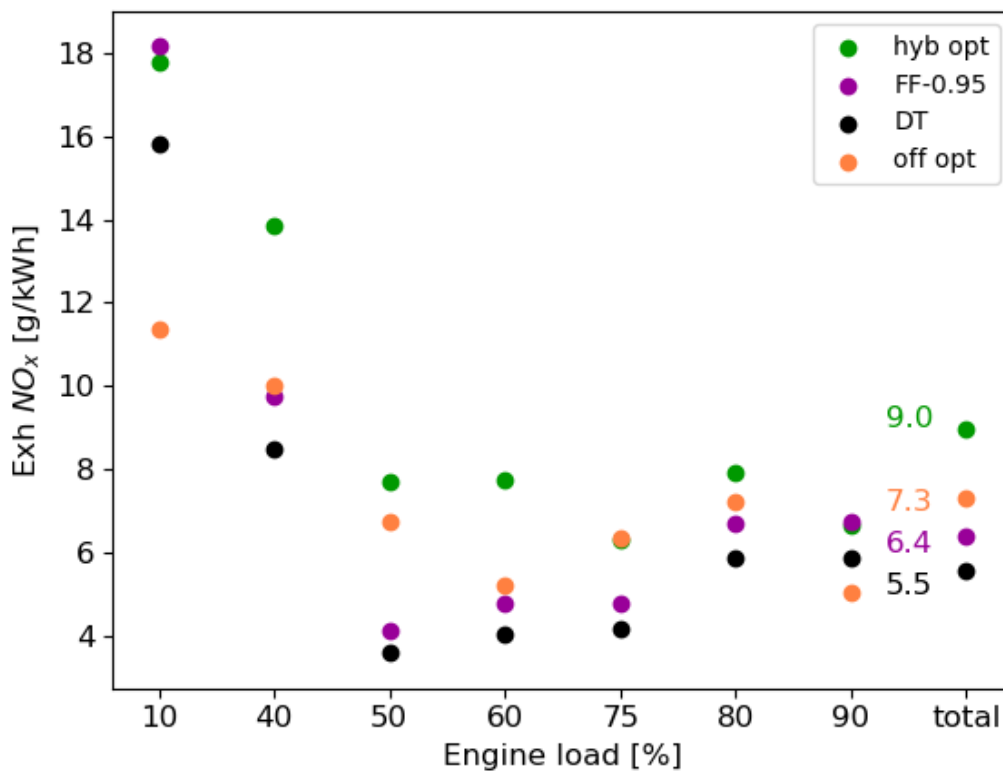


Figure 48: Exhaust NO_x emissions of the steady state load points and the average over the entire cycle



Figure 49 (a) and (b) show the average temperature at SCR inlet (a) and between the two SCR layers (b) for four different cycles. *DT* and *FF-0.95* were measured without any engine parameter changes (without any optimization) whereas *Off Opt* and *Hyb Opt* were offline and partly online optimized. From the data in Figure 49 it is obvious that the optimization heavily influenced the exhaust gas temperature. Since the current engine exhaust gas is at the lower limit of the catalyst, an increase of temperature is highly beneficiary for the catalyst. A higher exhaust gas temperature results in a higher activity of the catalyst. This directly influences the conversion efficiency, the NH_3 storage capacity and the agility of the catalyst. A higher SCR temperature is most advantageous in the low SCR temperature regime (below 300°C). The performance at 10% and 40% load was therefore enhanced most in the current set of samples.

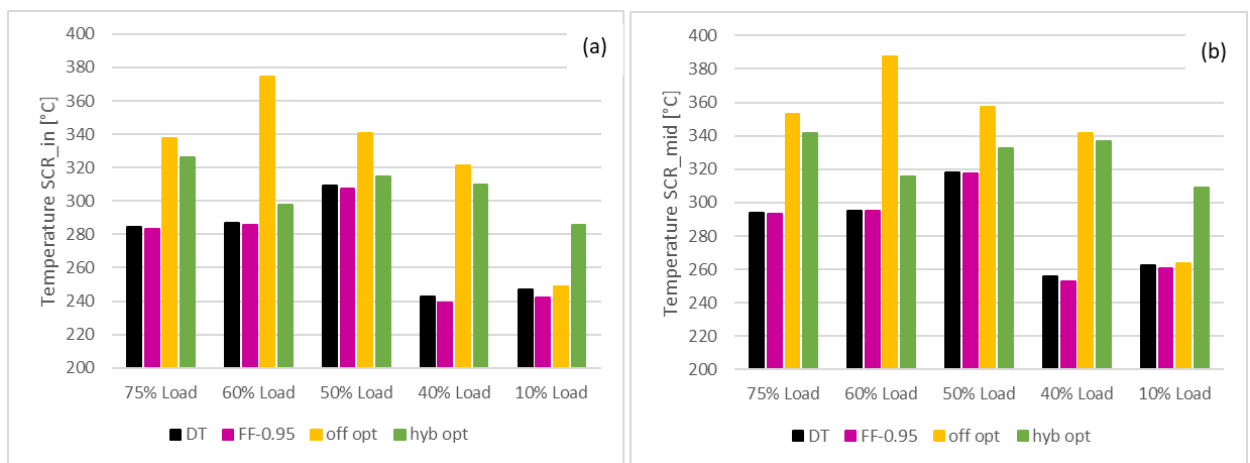


Figure 49: Temperature comparison at SCR inlet (a) and between the two layers (b) for the cycles *DT*, *FF-0.95*, *Off Opt* and *Hyb Opt*.



5 Conclusions

At PSI the large engine research facility and its exhaust aftertreatment system has been upgraded with a comprehensive installation to obtain information on the engine operation as well as the exhaust gas flow and SCR catalyst. All relevant data from various control and measurement systems is logged on a server to provide all involved parties data (e.g. PVS and Hug Control system) and control for the “Intelligent SCR” operation. This enables the observation of the SCR status with regard to its DeNO_x capability and the “Intelligent SCR” control system to adjust for its optimal operation at any time. An appropriate predication model for NO_x and NH₃ clean gas emissions in relation to engine out emission and operation conditions has been elaborated and calibrated by numerical optimization of model parameters retrieved by dedicated laboratory experiments.

In order to assess the performance of the novel “Intelligent SCR” system and its operation optimization a particular engine test cycle has been defined. This test cycle has been utilized to create a reference data set and afterwards, to evaluate and compare the results when operating the engine-SCR system with several control strategies. Along the project the complexity of the control system has been increased by incorporating further control system developments for the engine optimization, ranging from a lookup table, feedforward control to an optimized feedback approach. Thereby, the main optimization criteria are the fuel consumption, tail pipe NO_x emission (after SCR catalyst) and ammonia slip. This also included a virtual engine testbench to find the optimal operation conditions with regard to the set points of SOI, fuel pressure and WG position.

Overall, the optimized “Intelligent SCR” control system was able reduce fuel consumption by roughly 0.8% over the whole engine test cycle compared to the conventional look up dosing table control of the SCR system. The NO_x tail pipe emission was cut by about 50% and the ammonia slip is lowered by 60%. The novel interconnection of an advanced engine and SCR control system has proven its potential to reduce CO₂ emissions as well as significantly lowering the NO_x and ammonia slip.

The results presented in this project are highly interesting for medium and large engine system either used in land-based power generation systems or onboard of vessels as the environmental regulations are steadily increasing for such installations. Furthermore, the increase of renewable energies within the overall energy production landscape calls for solutions to master the accompanying difficulties of grid stability. Such engines systems could be part of the solution to provide energy for fast changing demand scenarios. Moreover, the project outcomes are presenting a technology potentially enabling a further reduction of GHG emissions to comply with the aims and goal of national as well as international treaties and agreements.



6 Outlook and next steps

Within this project the potential of the proposed technology “Intelligent SCR” has been elaborated and the highly promising results of the proof-of-concept lead to the continuation of the collaboration between PSI, Vir2sense and Hug Engineering. A grant for the Federal Office for the Environment (FOEN/BAFU) has been granted in order to further develop the optimized engine/SCR control system and to advance with the applicability of the technology. Hereby, the full implementation of the additional “Intelligent SCR” control system including also the online set point change of the SOI shall enhance the efficiency of the engine operation and the SCR system and hence, reducing CO₂, NO_x and ammonia emissions as well as the catalyst layout. All these aims and targets will be demonstrated at the large engine research facility at PSI.

Additionally, the virtual testbench has shown to be a valuable tool to produce the maps and the control strategies for the real tests. However, due to the yet limited access of the online available SOI control on the real engine, the full online optimized has been proofed to run on the testbench, but not with active control of SOI and WG. Figure 50 shows a comparison of online optimized strategy (*On Opt*) with the *Hyb Opt* and the *DT* strategy on the virtual testbench. It is shown that the fuel consumption is similar or lower in case of the *On Opt* strategy.

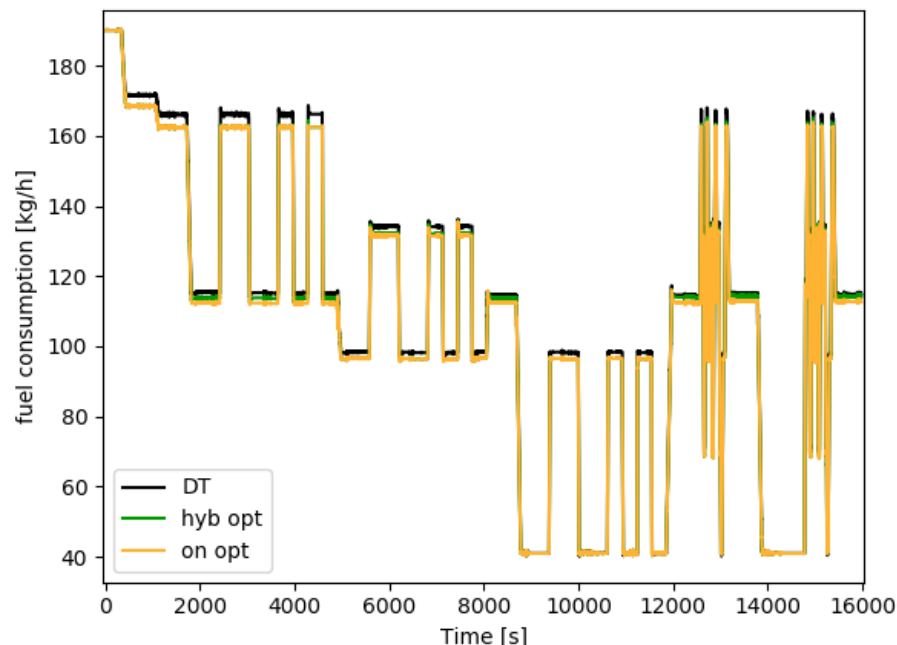


Figure 50: Fuel consumption simulation of the *DT*- (black), the *Hyb Opt*- (dark green) and the *On Opt* strategy (yellow) for the entire cycle.

Figure 51 shows a summary of the cycle relative to the *DT* strategy. The majority of the gain in fuel consumption is expected at 50% and 60% load. The overall estimation of the fuel consumption reduction is a bit exaggerated comparing the *Hyb Opt* and the *DT* strategy with the measurements. However, the



On Opt strategy in comparison to the *Hyb Opt* is expected to reduce the fuel consumption of the cycle by additionally approx. 0.5%.

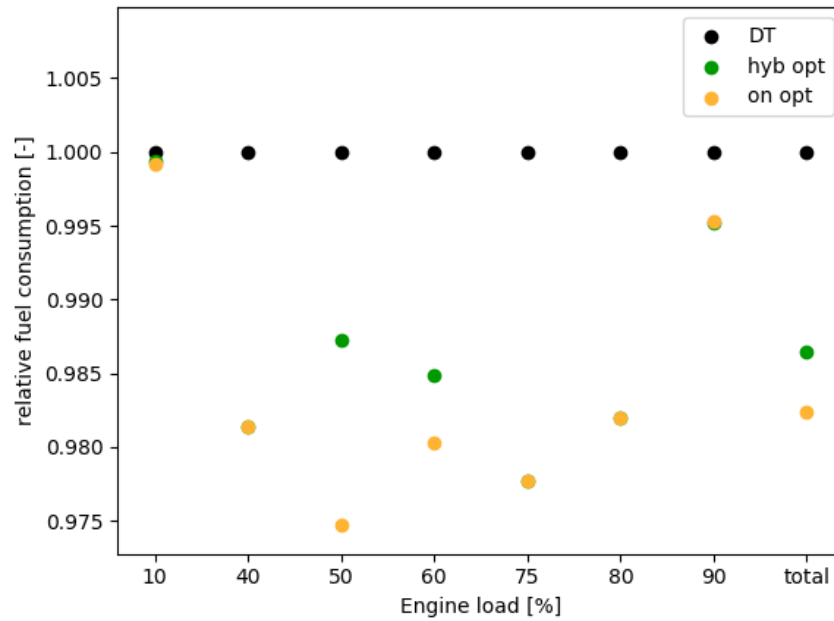


Figure 51: Fuel consumption of the *Hyb Opt* (dark green) and *On Opt* strategy (yellow) relative to the *DT* strategy (black), simulated with the virtual test bench. Load individual steady state parts of the cycle and average over the entire cycle.

This strategy will be tested in future campaigns.



7 National and international cooperation

The LERF facility is property of the ETH domain and therefore, a close collaboration with the LAV at ETH is given. Vir2sense is also in close collaboration with the LAV as the company is a spin-off of this laboratory. Furthermore, the FHNW is a close partner of the LERF and is also member of the LERF steering committee.

Additionally, all partners have cooperation with Swiss and international industrial partners such as ABB Turbo Systems, Kistler, Wärtsilä, WinGD etc.

8 Publications

- “Development and Application of a Physically Assisted Virtual Sensor (PVS) for NO_x Emissions”, P. Kyratos, C. Barro and B. von Rotz, CIMAC 2019, Vancouver, Jun2 2019
- Annual IEA Combustion TCP meeting in Montreux, 2019.

9 References

- [1] Kyratos, P., et al., "Recent developments in the Understanding of the Potential of In-Cylinder NO_x Reduction through Extreme Miller Valve Timing". CIMAC Congress 2013, 2013: p. Paper No.225.
- [2] Kyratos, P., et al., "Predictive Simulation and Experimental Validation of Phenomenological Combustion and Pollutant Models for Medium-Speed Common Rail Diesel Engines at Varying Inlet Conditions". CIMAC Congress 2010, 2010: p. Paper No. 143.
- [3] Kyratos, P., et al., "In-Cylinder Measurement Analysis of Diesel Engine Combustion with Miller Valve Timing". 13. Tagung "Der Arbeitsprozess des Verbrennungsmotors", 2011.
- [4] Kyratos, P., "The effects of prolonged ignition delay due to charge air temperature reduction on combustion in a diesel engine", 2013, Zürich: ETH.
- [5] Wik, C., et al., "2-stage Turbo Charging on Medium Speed Engines – Future Supercharging on the New LERF-Test Facility". 14. Aufladetechnische Konferenz, 2009.
- [6] Wik, C., et al., "2-stage turbo charging on medium speed engines – results from the LERF-test facility". 16. Aufladetechnische Konferenz, 2011.
- [7] Kyratos, P., et al., "Combination of EGR and Fuel-Water-Emulsions for Simultaneous NO_x and Soot Reduction in a Medium Speed Diesel Engine", CIMAC Congress 2016, 2016: p. Paper No. 248
- [8] B. von Rotz, P. Kyratos, K. Herrmann, K. Boulouchos, „Investigation of the Combined Application of Water-in-Fuel Emulsion and Exhaust Gas Recirculation in a Medium Speed Diesel Engine, CO-MODIA 2017, Okayama, Japan, 2017.